
Contents

1	Introduction	3
2	Model of geometrically nonlinear 3-D beam	5
2.1	Basic assumptions	5
2.2	Kinematic description of motion	5
2.3	Deformation	8
2.4	Constitutive equation	10
2.5	Elastic forces	10
2.6	Equation of motion	13
2.7	Incremental parameters	13
2.8	Time integration	14
2.9	Static solution	15
2.10	Stiffness matrices	16
2.10.1	Elastic stiffness	17
2.10.2	Geometric stiffness	18
2.10.3	Load-dependent stiffness matrix	21
2.11	Mass matrix and gyroscopic matrix	21
2.11.1	Consistent mass matrix	23
2.11.2	Lumped mass matrix	25
2.12	Damping matrix	26
2.13	Modal analysis	26
2.14	Buckling analysis	27
2.15	Frictionless contact	28
2.15.1	Formulation of tieline force	28
2.15.2	Frictional contact	29
2.16	Drilling fluid effects	30
2.16.1	Added mass matrix	30
2.16.2	Fluid-drag damping matrix	31
2.17	Steady-state motion	32
2.17.1	Critical RPM	33
3	Verification	35
3.1	Linear buckling	35
3.1.1	Buckling under compressive loads	35
3.1.2	Torsional buckling	35
3.2	Modal analysis	36
3.2.1	Torsional vibration of drill pipe with collar	36
3.2.2	Axially prestressed column	38
3.3	Static large-deflection analysis	40
3.3.1	Circular-arc cantilever	40

	Contents	1
3.4	Transient vibration	41
3.4.1	Beam with time-dependent axial force	41
3.4.2	Dynamics of spinning beams	41
3.4.3	Finite-amplitude dynamic deformation	45
4	BHA representation	47
4.1	Coordinate system	47
	References	49
	Index	51

Model of geometrically nonlinear 3-D beam

2.1 Basic assumptions

1. The beam is of uniform cross-section (prismatic).
2. The beam is slender and the Euler-Bernoulli assumption of cross-sectional planes remaining orthogonal to the deformed beam axis is sufficiently realistic.
3. The shear center of the beam coincides with the centroid of the cross-section, and the axes of the element frame are the principal directions of the cross-section. The twist is uncoupled from the flexure, which is true for doubly-symmetric cross-sections.
4. The cross-section of the beam is solid, or thin-walled but closed.
5. The cross-section of the beam does not deform in its plane.
6. Warping of the cross-section plane is negligible.
7. The individual beam elements remain close to straight throughout the deformation. The relative rotations of the cross-sections at the ends of the beam remain small.
8. The displacements of the nodes and the rotations of the cross-sections are not limited in magnitude.
9. The strains remain small throughout the deformation.
10. The response of the material is linear elastic.

2.2 Kinematic description of motion

The treatment of large deformation kinematics as described below follows the procedure of Krysl [6]. The motion of the beam is described by the locations of its nodes I and J , $\mathbf{x}^{(I)}$ and $\mathbf{x}^{(J)}$, and by the orientation of the nodal frame (triple of mutually orthogonal unit vectors) at each node, $\mathbf{R}^{(I)}$ and $\mathbf{R}^{(J)}$ (refer to Figure 2.1). The frame vectors $\mathbf{e}_k^{(M)}$, where $M = I, J$ and $k = 1, 2, 3$ are arranged as columns of an orthogonal (rotation) matrix

$$[\mathbf{R}^{(M)}] = \left[[\mathbf{e}_1^{(M)}], [\mathbf{e}_2^{(M)}], [\mathbf{e}_3^{(M)}] \right] . \quad (2.1)$$

By the notation $[\mathbf{e}_k^{(M)}]$ we mean the matrix of the components of the quantity in the bracket; if we don't say explicitly otherwise, the global Cartesian basis is understood.

These four parameters are changing in time, and they are referred to as the configuration of the beam. At the initial time instant $t = 0$ the configuration is ${}^0\mathcal{C}$, at some later time the configuration is ${}^t\mathcal{C}$. If we wish to distinguish at which time the configuration is taken we would use a superscript, for instance ${}^t\mathbf{x}^{(I)}$.

Initial configuration.

The locations of the two nodes of the beam element are given at the time $t = 0$ as data. The nodal frames at the time $t = 0$ consist of the Cartesian global vectors, and the matrix representing the nodal frame at that time is the identity matrix

$$[{}^0\mathbf{R}^{(M)}] = \left[\begin{bmatrix} 1 \\ 0 \\ 0 \end{bmatrix}, \begin{bmatrix} 0 \\ 1 \\ 0 \end{bmatrix}, \begin{bmatrix} 0 \\ 0 \\ 1 \end{bmatrix} \right].$$

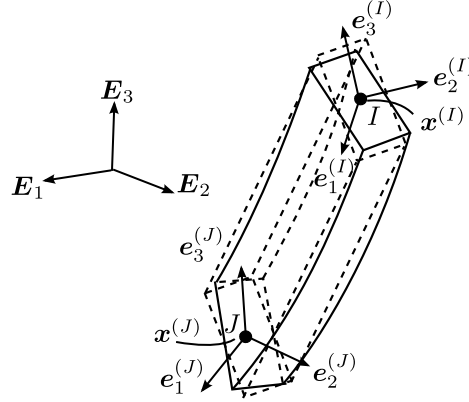


Fig. 2.1. Configuration parameters of a beam element

Corotational coordinate system in the initial configuration.

In addition to the global Cartesian coordinate system we will describe the deformation of the beam in a corotational coordinate system. This coordinate system is carried along by the beam, and it is described by the element frame (triple of orthogonal unit vectors) \mathbf{f}_k . The element frame is at any point in time defined by reference to the configuration of the beam— see Figure 2.2 for illustration.

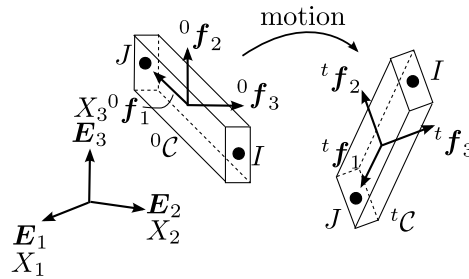


Fig. 2.2. Corotational coordinate systems used to track the motion of a beam element

At time $t = 0$ the element frame is determined by the input data. The first frame vector is defined as

$${}^0\mathbf{f}_1 = \frac{{}^0\mathbf{x}^{(J)} - {}^0\mathbf{x}^{(I)}}{\|{}^0\mathbf{x}^{(J)} - {}^0\mathbf{x}^{(I)}\|}. \quad (2.2)$$

The plane spanned by the vectors ${}^0\mathbf{f}_1$ and ${}^0\mathbf{f}_2$ is determined by the input vector $\mathbf{v}_{1,2}$. *Note that this vector must not be parallel to the axis of the beam in the initial configuration!* Using ${}^0\mathbf{f}_1$ and $\mathbf{v}_{1,2}$ the third vector of the element frame in the initial configuration is determined as the cross product

$${}^0\mathbf{f}_3 = \frac{{}^0\mathbf{f}_1 \times \mathbf{v}_{1,2}}{\|{}^0\mathbf{f}_1 \times \mathbf{v}_{1,2}\|},$$

and finally the second vector of the element frame and initial configuration is determined as the cross product

$${}^0\mathbf{f}_2 = {}^0\mathbf{f}_3 \times {}^0\mathbf{f}_1.$$

Note that the vectors ${}^0\mathbf{f}_2$ and ${}^0\mathbf{f}_3$ point in the *principal directions* of the cross-section. In other words, the element corotational frame is in the initial configuration located at the centroid of the cross-section, and the two coordinate axes in the cross-sectional plane are the principal axes of the cross-section.

Cross-section frames.

The orientations of the beam cross-sections at the nodes are defined by the cross-section frames. In the initial configuration the cross-section frames ${}^0\mathbf{f}_k^{(M)}$ are the same as the element frame

$${}^0\mathbf{f}_k^{(M)} = {}^0\mathbf{f}_k. \quad (2.3)$$

At any future time the orientation of the cross-section frame is determined by the motion of the node to which the cross-section is attached. We write

$${}^t\mathbf{f}_k^{(M)} = {}^t\mathbf{R}^{(M)} \cdot {}^0\mathbf{f}_k^{(M)}. \quad (2.4)$$

In words, the cross-section frames are rotated by the nodal rotation matrix. The cross-section frames are used to describe the orientation of the corotational element frame, and also the natural deformations of the beam (see Figure 2.3).

Corotational element frame at time t .

The corotational frame at any later time instant is not uniquely determined. Here we use the approach of Krysl [6]. The vector ${}^t\mathbf{f}_1$ is determined by the location of the nodes:

$${}^t\mathbf{f}_1 = \frac{{}^t\mathbf{x}^{(J)} - {}^t\mathbf{x}^{(I)}}{\|{}^t\mathbf{x}^{(J)} - {}^t\mathbf{x}^{(I)}\|}. \quad (2.5)$$

The third vector of the element frame is determined as the cross product

$${}^t\mathbf{f}_3 = {}^t\mathbf{f}_1 \times \frac{{}^t\mathbf{f}_2^{(I)} + {}^t\mathbf{f}_2^{(J)}}{\|{}^t\mathbf{f}_2^{(I)} + {}^t\mathbf{f}_2^{(J)}\|}. \quad (2.6)$$

Note that $({}^t\mathbf{f}_2^{(I)} + {}^t\mathbf{f}_2^{(J)})/2$ is the average of the cross-section frame vectors that were initially in the coordinate plane spanned by ${}^0\mathbf{f}_1$ and ${}^0\mathbf{f}_2$. As the beam twists the vectors ${}^t\mathbf{f}_2^{(I)}, {}^t\mathbf{f}_2^{(J)}$ lose their parallel orientation, but as long as the beam deformation is relatively small these two vectors still generally point in similar directions. Finally the second vector of the element frame in the configuration for time t is determined as the cross product

$${}^t\mathbf{f}_2 = {}^t\mathbf{f}_3 \times {}^t\mathbf{f}_1.$$

Compare the formulas above with Figure 2.3. For the purpose of transformation of quantities between the global Cartesian coordinates and the element frame the matrix that collects the frame basis vectors as columns

$${}^t\mathbf{F} = [{}^t\mathbf{f}_1, {}^t\mathbf{f}_2, {}^t\mathbf{f}_3] \quad (2.7)$$

will be referenced in further developments below.

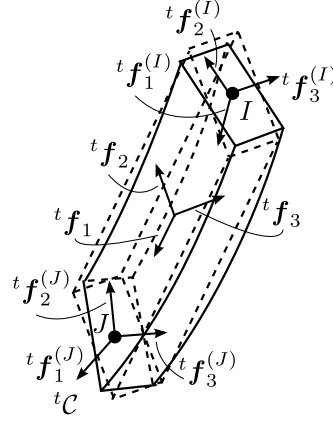


Fig. 2.3. Cross-section frames and the element frame in configuration ${}^t\mathcal{C}$

2.3 Deformation

Deformation is measured in the corotational element frame. Six of the so-called natural deformations are used to define unambiguously the strain-producing modes of stretching, bending, and twisting of the beam [3]. Figure 2.4 illustrates the six deformation modes, stretching d_{N1} , symmetric bending in the 1,2 plane d_{N2} , anti-symmetric bending in the 1,2 plane d_{N3} , symmetric bending in the 1,3 plane d_{N4} , anti-symmetric bending in the 1,3 plane d_{N5} , and twisting about the axis of the beam d_{N6} .

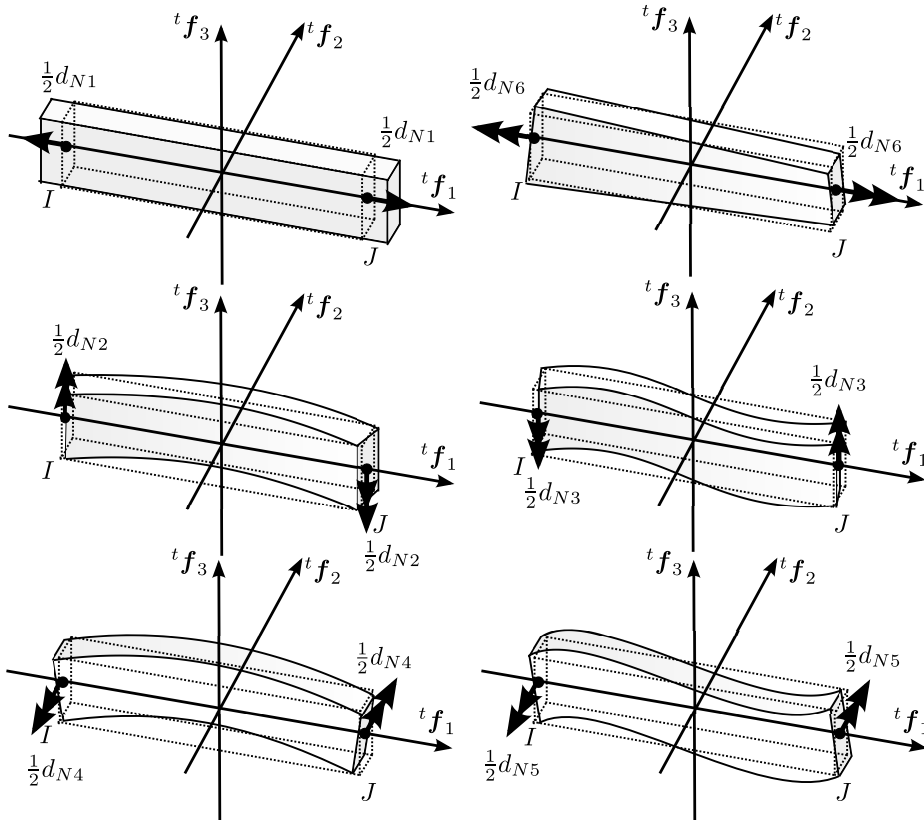


Fig. 2.4. Natural deformations in configuration ${}^t\mathcal{C}$

Stretching.

The stretching deformation is simply measured by the change in the distance between the two nodes of the element

$$d_{N1} = {}^tL - {}^0L, \quad (2.8)$$

where

$${}^0L = \|{}^0\mathbf{x}^{(J)} - {}^0\mathbf{x}^{(I)}\| \quad \text{and} \quad {}^tL = \|{}^t\mathbf{x}^{(J)} - {}^t\mathbf{x}^{(I)}\|.$$

Bending.

The bending deformation is described by the relative rotation of the cross-section frames with respect to the element frame. For small rotation angles the angle itself may be replaced by the tangent of the angle, which in turn may be expressed using the components of the cross-section frames in the element frame [6]. Bending deformation is determined by the components of the vector ${}^t\mathbf{f}_1^{(M)}$. Therefore, we compute the deformational rotation of node M about the element frame vector ${}^t\mathbf{f}_3$ as (positive rotation is determined by the right hand side rule)

$$\vartheta_3^{(M)} = + \frac{{}^t\mathbf{f}_2 \cdot {}^t\mathbf{f}_1^{(M)}}{{}^t\mathbf{f}_1 \cdot {}^t\mathbf{f}_1^{(M)}}, \quad (2.9)$$

and consequently the symmetric bending natural deformation is

$$d_{N2} = \vartheta_3^{(I)} - \vartheta_3^{(J)}. \quad (2.10)$$

The anti-symmetric bending natural deformation is

$$d_{N3} = \vartheta_3^{(I)} + \vartheta_3^{(J)}. \quad (2.11)$$

Similarly, we compute the deformational rotation of node M about the element frame vector ${}^t\mathbf{f}_2$ as

$$\vartheta_2^{(M)} = - \frac{{}^t\mathbf{f}_3 \cdot {}^t\mathbf{f}_1^{(M)}}{{}^t\mathbf{f}_1 \cdot {}^t\mathbf{f}_1^{(M)}}, \quad (2.12)$$

and the symmetric bending natural deformation is

$$d_{N4} = -\vartheta_2^{(I)} + \vartheta_2^{(J)}, \quad (2.13)$$

and the anti-symmetric bending natural deformation is

$$d_{N5} = -\vartheta_2^{(I)} - \vartheta_2^{(J)}. \quad (2.14)$$

Twisting.

Twisting deformation is computed by averaging the relative rotations about the axis of the beam between the pairs of vectors ${}^t\mathbf{f}_2^{(I)}, {}^t\mathbf{f}_2^{(J)}$ and ${}^t\mathbf{f}_3^{(I)}, {}^t\mathbf{f}_3^{(J)}$ to remove possible bias. The twisting natural deformation is computed as

$$2d_{N6} = \frac{{}^t\mathbf{f}_3 \cdot {}^t\mathbf{f}_2^{(J)}}{{}^t\mathbf{f}_2 \cdot {}^t\mathbf{f}_2^{(J)}} - \frac{{}^t\mathbf{f}_3 \cdot {}^t\mathbf{f}_2^{(I)}}{{}^t\mathbf{f}_2 \cdot {}^t\mathbf{f}_2^{(I)}} - \frac{{}^t\mathbf{f}_2 \cdot {}^t\mathbf{f}_3^{(J)}}{{}^t\mathbf{f}_3 \cdot {}^t\mathbf{f}_3^{(J)}} + \frac{{}^t\mathbf{f}_2 \cdot {}^t\mathbf{f}_3^{(I)}}{{}^t\mathbf{f}_3 \cdot {}^t\mathbf{f}_3^{(I)}}. \quad (2.15)$$

Note that whenever convenient we order the natural deformations into a vector \mathbf{d}_N

$$\mathbf{d}_N = [d_{Nj}].$$

2.4 Constitutive equation

The natural forces are produced by the natural deformations by applying the constitutive equation. Only linear elasticity is currently incorporated. The natural deformation modes are described within the element using cubic Hermite interpolation (the well-known cubic basis functions), and therefore the constitutive equation links the natural forces \mathbf{P}_N to the natural deformations via a diagonal matrix [3]

$$\mathbf{D}_N = \begin{bmatrix} \frac{EA}{L} & 0 & 0 & 0 & 0 & 0 \\ 0 & \frac{EI_3}{L} & 0 & 0 & 0 & 0 \\ 0 & 0 & \frac{3EI_3}{L} & 0 & 0 & 0 \\ 0 & 0 & 0 & \frac{EI_2}{L} & 0 & 0 \\ 0 & 0 & 0 & 0 & \frac{3EI_2}{L} & 0 \\ 0 & 0 & 0 & 0 & 0 & \frac{GJ}{L} \end{bmatrix}, \quad (2.16)$$

where L is the length of the element in the current configuration, E is the Young's modulus, G is the shear modulus, A is the cross-sectional area, I_2 and I_3 are the principal moments of inertia for bending about the centroid axes given by direction \mathbf{f}_3 and \mathbf{f}_2 respectively, and J is the St. Vénant torsion constant.

The natural forces are related to the natural deformations through the equation

$$\mathbf{P}_N = \mathbf{D}_N \mathbf{d}_N.$$

Call for Figure 2.5 and note the correspondence with the natural deformations from Figure 2.4.

2.5 Elastic forces

The internal forces (resultants of elastic stresses) in the cross-section the normal of which points along ${}^t\mathbf{f}_1$ (refer to Figure 2.6) are obtained from the natural forces (in the absence of distributed loads) as

$$N = P_{N1} \quad (2.17)$$

for the normal force N ,

$$S_2 = -\frac{2}{L}P_{N3}, \quad S_3 = -\frac{2}{L}P_{N5} \quad (2.18)$$

for the shear forces S_k , where S_k is positive if it points in the direction ${}^t\mathbf{f}_k$,

$$M_2 = P_{N4} - \frac{2x_1}{L}P_{N5}, \quad M_3 = -\left(P_{N2} - \frac{2x_1}{L}P_{N3}\right) \quad (2.19)$$

for the bending moments M_k , where M_k is positive if it turns according to the right-hand-side rule around the vector ${}^t\mathbf{f}_k$, and finally

$$M_1 = P_{N6} \quad (2.20)$$

for the twisting (torsional) moment M_1 , where M_1 is positive if it turns according to the right-hand-side rule around the vector ${}^t\mathbf{f}_1$. In the above, $-L/2 \leq x_1 \leq L/2$ is the coordinate along the centroid axis of the beam.

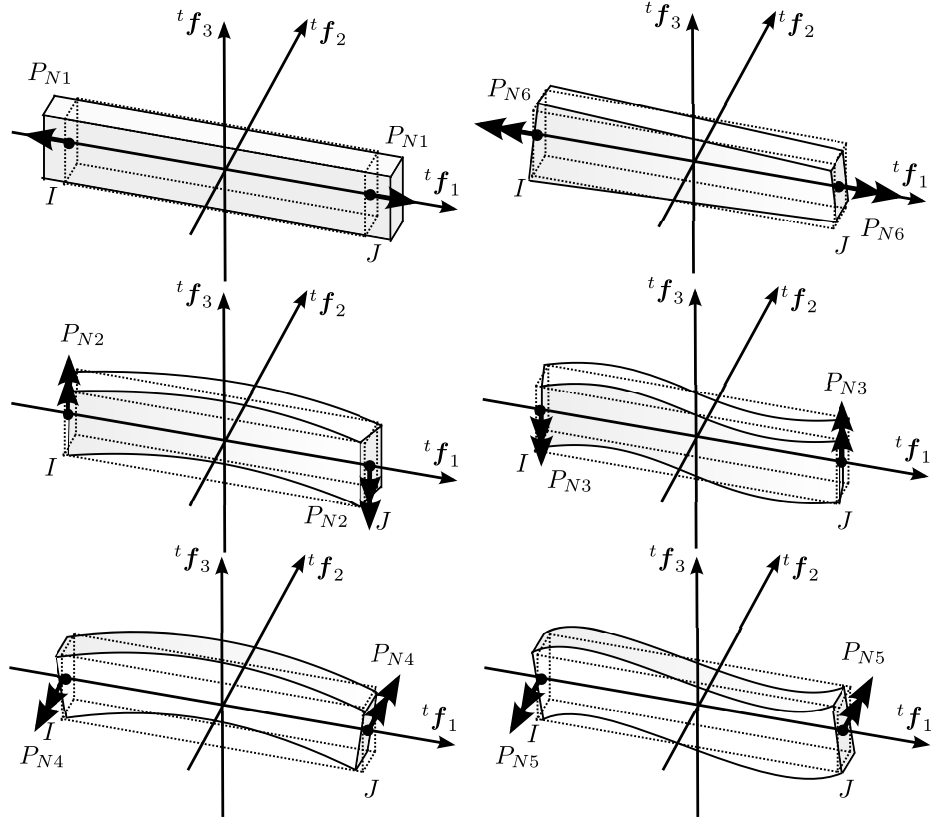


Fig. 2.5. Natural forces in configuration ${}^t\mathcal{C}$

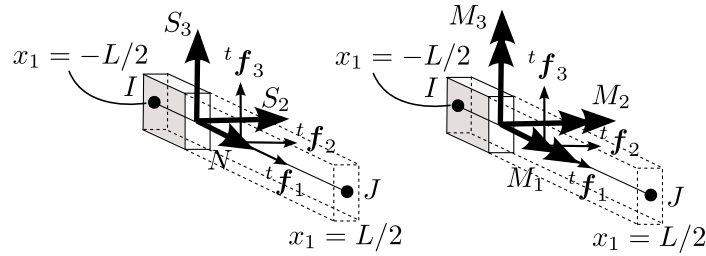


Fig. 2.6. Internal resultants in the beam cross-section

Cartesian components in the element frame.

The natural forces may thus be related to Cartesian forces and moments at the nodes. This relationship may be expressed using the so-called static matrix \mathbf{a}_N^T [3]

$$\mathbf{a}_N^T = \begin{bmatrix} -1 & 0 & 0 & 0 & 0 & 0 \\ 0 & 0 & 2/L & 0 & 0 & 0 \\ 0 & 0 & 0 & 0 & 2/L & 0 \\ 0 & 0 & 0 & 0 & 0 & -1 \\ 0 & 0 & 0 & -1 & -1 & 0 \\ 0 & 1 & 1 & 0 & 0 & 0 \\ 1 & 0 & 0 & 0 & 0 & 0 \\ 0 & 0 & -2/L & 0 & 0 & 0 \\ 0 & 0 & 0 & 0 & -2/L & 0 \\ 0 & 0 & 0 & 0 & 0 & 1 \\ 0 & 0 & 0 & 1 & -1 & 0 \\ 0 & -1 & 1 & 0 & 0 & 0 \end{bmatrix}, \quad (2.21)$$

yielding

$$\mathbf{P}_{(f)} = \mathbf{a}_N^T \mathbf{P}_N. \quad (2.22)$$

The components are labeled $P_{(f)j}$ to indicate that the components are on the frame basis vectors ${}^t\mathbf{f}_k$.

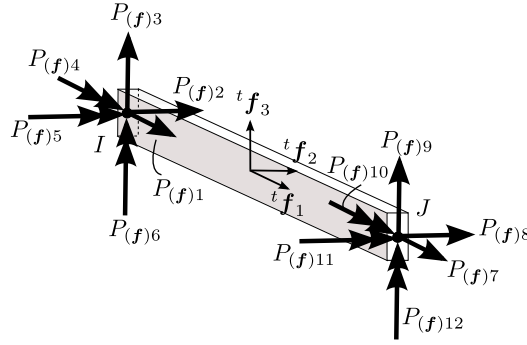


Fig. 2.7. Cartesian components of forces and moments at the nodes $P_{(f)j}$ in the element frame ${}^t\mathbf{f}_k$

Global Cartesian components.

The transformation from the corotational element frame forces to forces in the global Cartesian coordinate system \mathbf{P} is a rotation

$$\mathbf{P} = \begin{bmatrix} \mathbf{F} & \mathbf{0} & \mathbf{0} & \mathbf{0} \\ \mathbf{0} & \mathbf{F} & \mathbf{0} & \mathbf{0} \\ \mathbf{0} & \mathbf{0} & \mathbf{F} & \mathbf{0} \\ \mathbf{0} & \mathbf{0} & \mathbf{0} & \mathbf{F} \end{bmatrix} \mathbf{P}_{(f)} = \mathbf{T} \mathbf{P}_{(f)}. \quad (2.23)$$

The transformation matrix \mathbf{T} is called the elementwise rotation matrix, and consists of the four blocks on the diagonal which are the element-frame matrices. The matrix of components of the element frame \mathbf{F} of (2.7) in the global Cartesian coordinates consists of column matrices of the components of the element frame basis vectors

$$[\mathbf{F}] = [[\mathbf{f}_1], [\mathbf{f}_2], [\mathbf{f}_3]].$$

The transformation (2.23) may be inverted to yield

$$\mathbf{P}_{(f)} = \mathbf{T}^T \mathbf{P}. \quad (2.24)$$

Restoring force.

The vector \mathbf{P} is the vector of forces and moments that act on the element. The forces equal to \mathbf{P} in magnitude but opposite in direction are the restoring forces, $\mathbf{r} = -\mathbf{P}$. These are the forces by which the elements act on the nodes, resisting the deformation, attempting to restore the structure to an undeformed state.

2.6 Equation of motion

After the individual element matrices are assembled the global system of equations of motion is obtained as

$$\mathbf{M}\mathbf{a} = \mathbf{L} + \mathbf{r}(\boldsymbol{\chi}) - \tilde{\mathbf{C}}\mathbf{v} , \quad (2.25)$$

where \mathbf{M} is the mass matrix, \mathbf{a} are the accelerations, $\tilde{\mathbf{C}}$ is the “damping” matrix (which may produce non-damping velocity-proportional effects such as the gyroscopic force), \mathbf{v} are the velocities, \mathbf{L} is a vector of external loads (forces and torques), and \mathbf{r} is the vector of restoring forces.

The configuration parameters $\boldsymbol{\chi} = \{\mathbf{u}^{(J)}, \mathbf{R}^{(J)}\}$ are the displacements of the nodes $\mathbf{u}^{(J)}$ and the nodal frames $\mathbf{R}^{(J)}$ for all nodes J in the mesh.

Note that the load vector may depend on time, and the vector of restoring forces depends on the configuration parameters. In addition, the mass and damping matrix also depend on the configuration parameters implicitly due to the continuously changing orientations of the element frames. Refer to following sections for details pertaining to the calculation of the various matrices.

In equation (2.25) the left-hand side are the inertial forces, and on the right-hand side there are the external loads, the elastic restoring forces, and the damping forces. In the state of static deformation, the absence of velocities and accelerations reduces the equation of motion to

$$\mathbf{L}(t) + \mathbf{r}(\boldsymbol{\chi}) = \mathbf{0} \quad (2.26)$$

which is a nonlinear algebraic equation for the unknown configuration parameters. This equation is typically solved with Newton-Raphson iteration described in Section 2.9.

For time-dependent deformation processes the most general option is direct time integration described in Section 2.8.

2.7 Incremental parameters

The use of incremental configuration parameters will be explained on the case of the equation of static deformation. For some value of the loading parameter $t = {}^n t$ the configuration parameters are known ${}^n \boldsymbol{\chi}$, and the solution is sought for a close-by loading parameter value $t = {}^{n+1} t$. The Newton-Raphson procedure is based on the expansion

$$\mathbf{L}({}^n t) + \mathbf{r}({}^n \boldsymbol{\chi}) + D(\mathbf{L}({}^n t) + \mathbf{r}({}^n \boldsymbol{\chi}))[\Delta \boldsymbol{\chi}] \approx \mathbf{0} ,$$

where $D(\mathbf{L}({}^n t) + \mathbf{r}({}^n \boldsymbol{\chi}))[\Delta \boldsymbol{\chi}]$ is the directional derivative. The vector $\Delta \boldsymbol{\chi}$ is the linear part of the change of the configuration parameters. This increment is solved for from the above equation and the repeated application of the formula leads to the Newton-Raphson iteration that is continued until some tolerance is met.

For the displacements of the nodes, the linear part of the change of the configuration $\boldsymbol{\chi}$ is simply an incremental displacement $\Delta \mathbf{u}^{(J)}$

$$\mathbf{u}^{(J)} = {}^n \mathbf{u}^{(J)} + \Delta \mathbf{u}^{(J)} . \quad (2.27)$$

The configuration parameters that describe the orientation of the nodes, the nodal frames $\mathbf{R}^{(J)}$, are rotation matrices which are tricky to parameterize for motion of arbitrary-magnitude [3]. The problem is solved here using incremental parameterization [6]. The nodal frames $\mathbf{R}^{(J)}$ are evolved using incremental rotation matrices which are parameterized with incremental axial rotation vectors

$$\mathbf{R}^{(J)} = \exp \left[\Delta \boldsymbol{\theta}^{(J)} \right] \cdot {}^n \mathbf{R}^{(J)} \quad (2.28)$$

The directional derivative of the nodal frame is

$$D\mathbf{R}^{(J)}[\Delta \boldsymbol{\theta}^{(J)}] = D \left(\exp \left[\Delta \boldsymbol{\theta}^{(J)} \right] \cdot {}^n \mathbf{R}^{(J)} \right) [\Delta \boldsymbol{\theta}^{(J)}] = \widetilde{\Delta \boldsymbol{\theta}^{(J)}} \cdot {}^n \mathbf{R}^{(J)}, \quad (2.29)$$

where $\widetilde{\Delta \boldsymbol{\theta}^{(J)}}$ is a skew-symmetric matrix that is equivalent to the vector cross product as

$$\widetilde{\Delta \boldsymbol{\theta}^{(J)}} \cdot \mathbf{w} = \Delta \boldsymbol{\theta}^{(J)} \times \mathbf{w} \quad \text{for arbitrary } \mathbf{w}. \quad (2.30)$$

Therefore, we can take the components of the incremental rotation vector as the parameterization of the rotation configuration variables, and the incremental configuration parameters are adopted here as

$$\Delta \boldsymbol{\chi} = \left\{ \Delta \mathbf{u}^{(J)}, \Delta \boldsymbol{\theta}^{(J)} \right\}. \quad (2.31)$$

The configuration is updated using (2.27) and (2.28) (in symbolic notation)

$$\boldsymbol{\chi} = \left\{ \mathbf{u}^{(J)}, \mathbf{R}^{(J)} \right\} \rightarrow \boldsymbol{\chi} + \Delta \boldsymbol{\chi} = \left\{ \mathbf{u}^{(J)} + \Delta \mathbf{u}^{(J)}, \exp \left[\Delta \boldsymbol{\theta}^{(J)} \right] \mathbf{R}^{(J)} \right\}. \quad (2.32)$$

The directional derivative may be therefore written as

$$D(\mathbf{L}({}^n \mathbf{t}) + \mathbf{r}({}^n \boldsymbol{\chi}))[\Delta \boldsymbol{\chi}] = \frac{\partial}{\partial \Delta \boldsymbol{\chi}} (\mathbf{L}({}^n \mathbf{t}) + \mathbf{r}({}^n \boldsymbol{\chi})) \cdot \Delta \boldsymbol{\chi}.$$

The partial derivative with respect to the increment of the configuration parameters leads to the tangent stiffness matrix as explained in Section 2.10.

2.8 Time integration

The time integration is handled with the Newmark algorithm reformulated as advocated in [6]. In particular, the rotation degrees of freedom are treated not as vector quantities, but the rotations are described by orthogonal rotation matrices (nodal frames). The nodal frames are updated by incremental rotations.

1. $t = 0$
2. while ($t \leq t_{end}$)
 - a) Initialize iteration:
 - i. ${}^{t+\Delta t, (0)} \boldsymbol{\chi} = {}^t \boldsymbol{\chi}$
 - ii. ${}^{t+\Delta t, (0)} \mathbf{a} = -\frac{1}{\gamma \Delta t} {}^t \mathbf{v} - \left(\frac{1}{2} - \beta \right) {}^t \mathbf{a}$
 - iii. ${}^{t+\Delta t, (0)} \mathbf{v} = {}^t \mathbf{v} + \Delta t \left[(1 - \gamma) {}^t \mathbf{a} + \gamma {}^{t+\Delta t, (0)} \mathbf{a} \right]$
 - iv. $\Delta^t \widehat{\Delta \boldsymbol{\chi}} = \Delta t {}^t \mathbf{v} + \frac{\Delta t^2}{2} (1 - 2\beta) {}^t \mathbf{a}$
 - v. ${}^{t+\Delta t} \widehat{\mathbf{v}} = {}^t \mathbf{v} + \Delta t (1 - \gamma) {}^t \mathbf{a}$
 - vi. $\Delta^t \Delta \boldsymbol{\chi} = \mathbf{0}$
 - vii. $j = 0$

- b) Iterate
- i. Assemble loads $\mathbf{L} = \mathbf{L}(t + \Delta t)$
 - ii. Assemble restoring force $\mathbf{r} = \mathbf{r}^{(t+\Delta t, (j))} \boldsymbol{\chi}$
 - iii. Assemble stiffness matrix $\mathbf{K} = \mathbf{K}^{(t+\Delta t, (j))} \boldsymbol{\chi}$
 - iv. Assemble mass matrix $\mathbf{M} = \mathbf{M}^{(t+\Delta t, (j))} \boldsymbol{\chi}$
 - v. Assemble damping matrix $\mathbf{C} = \mathbf{C}^{(t+\Delta t, (j))} \boldsymbol{\chi}$
 - vi. Assemble gyroscopic matrix $\mathbf{G} = \mathbf{G}^{(t+\Delta t, (j))} \boldsymbol{\chi}$
 - vii. Solve for configuration parameter increment from

$$\left(\mathbf{K} + \frac{\gamma}{\beta \Delta t} (\mathbf{C} + \mathbf{G}) + \frac{1}{\beta \Delta t^2} \mathbf{M} \right) \Delta \boldsymbol{\chi} = \mathbf{L} + \mathbf{r} + \frac{1}{\beta \Delta t^2} \mathbf{M} \left(-\Delta t \Delta \boldsymbol{\chi} + \Delta t \widehat{\Delta \boldsymbol{\chi}} \right) + \frac{\gamma}{\beta \Delta t} (\mathbf{C} + \mathbf{G}) \left(-\Delta t \Delta \boldsymbol{\chi} + \Delta t \widehat{\Delta \boldsymbol{\chi}} - \frac{\beta \Delta t}{\gamma} {}^{t+\Delta t} \widehat{\mathbf{v}} \right)$$
 - viii. Update configuration:
 - A. ${}^{t+\Delta t, (j+1)} \mathbf{u} = {}^{t+\Delta t, (j+1)} \mathbf{u} + \text{transl}[\Delta \boldsymbol{\chi}]$
 - B. ${}^{t+\Delta t, (j+1)} \mathbf{R} = \text{exp rotat}[\Delta \boldsymbol{\chi}] \cdot {}^{t+\Delta t, (j+1)} \mathbf{R}$
 - C. $\Delta t \Delta \boldsymbol{\chi} = \Delta t \Delta \boldsymbol{\chi} + \Delta \boldsymbol{\chi}$
 - D. ${}^{t+\Delta t, (j+1)} \mathbf{v} = {}^{t+\Delta t, (j+1)} \mathbf{v} + \frac{\gamma}{\beta \Delta t} \Delta \boldsymbol{\chi}$
 - E. ${}^{t+\Delta t, (j+1)} \mathbf{a} = {}^{t+\Delta t, (j+1)} \mathbf{a} + \frac{1}{\beta \Delta t^2} \Delta \boldsymbol{\chi}$
 - ix. If $\|\Delta \boldsymbol{\chi}\| \leq \text{Tolerance}$ then break iteration; otherwise $j = j + 1$ and continue
- c) Reset for the next time step:
- i. ${}^t \boldsymbol{\chi} = {}^{t+\Delta t, (j+1)} \boldsymbol{\chi}$
 - ii. ${}^t \mathbf{v} = {}^{t+\Delta t, (j+1)} \mathbf{v}$
 - iii. ${}^t \mathbf{a} = {}^{t+\Delta t, (j+1)} \mathbf{a}$
 - iv. $t = t + \Delta t$

Remarks:

1. The vector $\Delta \boldsymbol{\chi}$ collects the degrees of freedom for the nodes of the finite element model, both displacements and rotations.
2. The result of $\text{transl}[\Delta \boldsymbol{\chi}]$ should be understood as the extraction of the values of the degrees of freedom that correspond to translation of the nodes from the increment of the configuration.
3. The result of $\text{rotat}[\Delta \boldsymbol{\chi}]$ should be understood as the extraction of the values of the degrees of freedom that correspond to rotation of the nodes from the increment of the configuration.
4. The operation $\text{exp rotat}[\Delta \boldsymbol{\chi}] \cdot {}^{t+\Delta t, (j)} \mathbf{R}$ is a symbolic notation that stands for the application of incremental rotation matrices to each individual nodal frame. The incremental rotation matrices are computed from the rotation increment $\text{rotat}[\Delta \boldsymbol{\chi}]$.
5. The vector ${}^{t+\Delta t} \Delta \boldsymbol{\chi}$ collects the total vectorial increment within the time step, both for rotation and displacement of nodes.

2.9 Static solution

Time here has the meaning of the load parameter. For instance, the external load could be taken as nodal force $\mathbf{L}(t) = t \overline{\mathbf{L}}$, where $\overline{\mathbf{L}}$ is given spatial distribution of the load.

The response integration is handled as advocated in [6]. In particular, the rotation degrees of freedom are treated not as vector quantities, but the rotations are described by orthogonal rotation matrices (nodal frames). The nodal frames are updated by incremental rotations.

1. $t = 0$
2. while $(t \leq t_{\text{end}})$

- a) Initialize iteration:
 - i. ${}^{t+\Delta t,(0)}\mathbf{u} = {}^t\mathbf{u}$
 - ii. ${}^{t+\Delta t,(0)}\mathbf{R} = {}^t\mathbf{R}$
 - iii. $j = 0$
- b) Iterate
 - i. Assemble loads $\mathbf{L} = \mathbf{L}(t + \Delta t)$
 - ii. Assemble restoring force $\mathbf{r} = \mathbf{r}({}^{t+\Delta t,(j)}\mathbf{u}, {}^{t+\Delta t,(j)}\mathbf{R})$
 - iii. Assemble stiffness matrix $\mathbf{K} = \mathbf{K}({}^{t+\Delta t,(j)}\mathbf{u}, {}^{t+\Delta t,(j)}\mathbf{R})$
 - iv. Solve for configuration parameter increment from $\mathbf{K}\Delta\chi = \mathbf{L} + \mathbf{r}$
 - v. Update configuration:
 - A. ${}^{t+\Delta t,(j+1)}\mathbf{u} = {}^{t+\Delta t,(j)}\mathbf{u} + \text{transl}[\Delta\chi]$
 - B. ${}^{t+\Delta t,(j+1)}\mathbf{R} = \exp \text{rotat}[\Delta\chi] \cdot {}^{t+\Delta t,(j)}\mathbf{R}$
 - vi. If $\|\Delta\chi\| \leq \text{Tolerance}$ then break iteration; otherwise $j = j + 1$ and continue
- c) Reset for the next load step:
 - i. ${}^t\mathbf{u} = {}^{t+\Delta t,(j+1)}\mathbf{u}$
 - ii. ${}^t\mathbf{R} = {}^{t+\Delta t,(j+1)}\mathbf{R}$
 - iii. $t = t + \Delta t$

Remarks:

1. The vector $\Delta\chi$ collects the degrees of freedom for the nodes of the finite element model, both displacements and rotations.
2. The result of $\text{transl}[\Delta\chi]$ should be understood as the extraction of the values of the degrees of freedom that correspond to translation of the nodes from the increment of the configuration.
3. The result of $\text{rotat}[\Delta\chi]$ should be understood as the extraction of the values of the degrees of freedom that correspond to rotation of the nodes from the increment of the configuration.
4. The operation $\exp \text{rotat}[\Delta\chi] \cdot {}^{t+\Delta t,(j)}\mathbf{R}$ is a symbolic notation that stands for the application of incremental rotation matrices to each individual nodal frame. The incremental rotation matrices are computed from the rotation increment $\text{rotat}[\Delta\chi]$.

2.10 Stiffness matrices

The restoring force is linearized to express the increment of the forces as linearly dependent on the increment of the configuration parameters through the tangent stiffness matrix.

The restoring force acting upon the nodes by a single beam element may be linearized with the directional derivative by substituting the expression (2.23)

$$D(\mathbf{r}({}^n\chi)) \cdot \Delta\chi = D(-\mathbf{P}({}^n\chi)) \cdot \Delta\chi = D(-\mathbf{T}({}^n\chi) \mathbf{P}_{(f)}({}^n\chi)) \cdot \Delta\chi, \quad (2.33)$$

or, using the relationship between the Cartesian forces in the element frame and the natural forces (2.22), as

$$D(-\mathbf{T}({}^n\chi) \mathbf{P}_{(f)}({}^n\chi)) \cdot \Delta\chi = D(-\mathbf{T}({}^n\chi) \mathbf{a}_N^T({}^n\chi) \mathbf{P}_N({}^n\chi)) \cdot \Delta\chi. \quad (2.34)$$

Note that *all* quantities depend on the current configuration ${}^n\chi$. Keeping this in mind we shall drop the explicit reference to the current configuration and we will write

$$D(\mathbf{r}) \cdot \Delta\chi = D(-\mathbf{T} \mathbf{a}_N^T \mathbf{P}_N) \cdot \Delta\chi.$$

Applying the chain rule we may separate the directional derivative into two terms

$$D(\mathbf{T} \mathbf{a}_N^T \mathbf{P}_N) \cdot \Delta\chi = D(\mathbf{T} \mathbf{a}_N^T) \cdot \Delta\chi \mathbf{P}_N + \mathbf{T} \mathbf{a}_N^T D(\mathbf{P}_N) \cdot \Delta\chi. \quad (2.35)$$

The first term results in the so-called geometric stiffness matrix

$$D(\mathbf{T}({}^n\chi) \mathbf{a}_N^T({}^n\chi)) \cdot \Delta\chi \mathbf{P}_N({}^n\chi) = \mathbf{K}^G \Delta\chi,$$

and the second term results in the elastic stiffness matrix

$$\mathbf{T} \mathbf{a}_N^T D(\mathbf{P}_N) \cdot \Delta\chi = \mathbf{K}^E \Delta\chi.$$

2.10.1 Elastic stiffness

The directional derivative

$$\mathbf{T}\mathbf{a}_N^T D(\mathbf{P}_N) \cdot \Delta\boldsymbol{\chi} \quad (2.36)$$

may be evaluated using the constitutive equation for the natural forces to obtain

$$\mathbf{T}\mathbf{a}_N^T D(\mathbf{P}_N) \cdot \Delta\boldsymbol{\chi} = \mathbf{T}\mathbf{a}_N^T D(\mathbf{D}_N \mathbf{d}_N) \cdot \Delta\boldsymbol{\chi} , \quad (2.37)$$

which simplifies because the constitutive matrix is independent of deformation to

$$\mathbf{T}\mathbf{a}_N^T D(\mathbf{P}_N) \cdot \Delta\boldsymbol{\chi} = \mathbf{T}\mathbf{a}_N^T \mathbf{D}_N D(\mathbf{d}_N) \cdot \Delta\boldsymbol{\chi} . \quad (2.38)$$

The linearization of the natural deformations is yielded by the transpose of the static matrix (2.21) and the increment of the configuration parameters expressed on the element frame

$$D(\mathbf{d}_N) \cdot \Delta\boldsymbol{\chi} = \mathbf{a}_N \cdot \Delta\boldsymbol{\chi}_{(f)} , \quad (2.39)$$

or with the transformation (2.24)

$$D(\mathbf{d}_N) \cdot \Delta\boldsymbol{\chi} = \mathbf{a}_N \cdot \mathbf{T}^T \Delta\boldsymbol{\chi} , \quad (2.40)$$

and so we obtain

$$\mathbf{T}\mathbf{a}_N^T D(\mathbf{P}_N) \cdot \Delta\boldsymbol{\chi} = \mathbf{T}\mathbf{a}_N^T \mathbf{D}_N \mathbf{a}_N \mathbf{T}^T \cdot \Delta\boldsymbol{\chi} . \quad (2.41)$$

The square matrix

$$\mathbf{K}_{(f)}^E = \mathbf{a}_N^T \mathbf{D}_N \mathbf{a}_N \quad (2.42)$$

is the elastic stiffness of the beam in the element frame, and the elastic stiffness in the global basis is

$$\mathbf{K}^E = \mathbf{T} \mathbf{K}_{(f)}^E \mathbf{T}^T = \mathbf{T} \mathbf{a}_N^T \mathbf{D}_N \mathbf{a}_N \mathbf{T}^T . \quad (2.43)$$

The elastic stiffness in the element frame may be written explicitly as the four submatrices $\mathbf{K}_{(f),AB}^E$ of the elastic stiffness that link nodes $A = I, J$ and $B = I, J$

$$\mathbf{K}_{(f),II}^E = \begin{bmatrix} (AE)/L & 0 & 0 & 0 & 0 & 0 \\ 0 & (12EI_3)/L^3 & 0 & 0 & 0 & (6EI_3)/L^2 \\ 0 & 0 & (12EI_2)/L^3 & 0 & -(6EI_2)/L^2 & 0 \\ 0 & 0 & 0 & (GJ)/L & 0 & 0 \\ 0 & 0 & -(6EI_2)/L^2 & 0 & (4EI_2)/L & 0 \\ 0 & (6EI_3)/L^2 & 0 & 0 & 0 & (4EI_3)/L \end{bmatrix} \quad (2.44)$$

$$\mathbf{K}_{(f),IJ}^E = \begin{bmatrix} -(AE)/L & 0 & 0 & 0 & 0 & 0 \\ 0 & -(12EI_3)/L^3 & 0 & 0 & 0 & (6EI_3)/L^2 \\ 0 & 0 & -(12EI_2)/L^3 & 0 & -(6EI_2)/L^2 & 0 \\ 0 & 0 & 0 & -(GJ)/L & 0 & 0 \\ 0 & 0 & (6EI_2)/L^2 & 0 & (2EI_2)/L & 0 \\ 0 & -(6EI_3)/L^2 & 0 & 0 & 0 & (2EI_3)/L \end{bmatrix}$$

$$(2.45)$$

$$K_{(\mathbf{f}),JI}^E = K_{(\mathbf{f}),IJ}^E{}^T \quad (2.46)$$

and finally

$$K_{(\mathbf{f}),JJ}^E = \begin{bmatrix} (AE)/L & 0 & 0 & 0 & 0 & 0 \\ 0 & (12EI_3)/L^3 & 0 & 0 & 0 & -(6EI_3)/L^2 \\ 0 & 0 & (12EI_2)/L^3 & 0 & (6EI_2)/L^2 & 0 \\ 0 & 0 & 0 & (GJ)/L & 0 & 0 \\ 0 & 0 & (6EI_2)/L^2 & 0 & (4EI_2)/L & 0 \\ 0 & -(6EI_3)/L^2 & 0 & 0 & 0 & (4EI_3)/L \end{bmatrix}. \quad (2.47)$$

2.10.2 Geometric stiffness

The linearization of the first term in (2.35) results in the so-called geometric stiffness matrix

$$D(\mathbf{T}({}^n\boldsymbol{\chi}) \mathbf{a}_N^T({}^n\boldsymbol{\chi})) \cdot \Delta\boldsymbol{\chi} \mathbf{P}_N({}^n\boldsymbol{\chi}) = \mathbf{K}^G \Delta\boldsymbol{\chi}.$$

Again, the dependence on the current configuration will be omitted for the sake of brevity. The product of the rotation matrix (2.23) and the static matrix may be expanded into

$$\mathbf{T} \mathbf{a}_N^T = \begin{bmatrix} -\mathbf{f}_1, & \mathbf{0}, & \frac{2}{L}\mathbf{f}_2, & \mathbf{0}, & \frac{2}{L}\mathbf{f}_3, & \mathbf{0} \\ \mathbf{0} & \mathbf{f}_3, & \mathbf{f}_3 - \mathbf{f}_2, & -\mathbf{f}_2 - \mathbf{f}_1 \\ \mathbf{f}_1, & \mathbf{0}, & -\frac{2}{L}\mathbf{f}_2, & \mathbf{0}, & -\frac{2}{L}\mathbf{f}_3, & \mathbf{0} \\ \mathbf{0}, & -\mathbf{f}_3, & \mathbf{f}_3, & \mathbf{f}_2, & -\mathbf{f}_2, & \mathbf{f}_1 \end{bmatrix} \quad (2.48)$$

The purpose of the linearization of $D(\mathbf{T} \mathbf{a}_N^T) \cdot \Delta\boldsymbol{\chi}$ is to express the rotation of the element frame basis vectors due to the incremental configuration parameters and the change of the element length. The directional derivative with respect to the change in length is

$$D(1/L)[\Delta L] = -\Delta L/L^2$$

and the incremental rotation of the element frame is

$$D(\mathbf{f}_k)[\Delta\boldsymbol{\psi}] = \Delta\boldsymbol{\psi} \times \mathbf{f}_k$$

where the incremental rotation of the element frame $\Delta\boldsymbol{\psi}$ is due to the average of the axial rotations and the rotation due to the differences of the transverse displacements (refer to Figure 2.7 where an obvious visual substitution is made to replace the force components $P_{(\mathbf{f})j}$ with the incremental displacements $\Delta\chi_{(\mathbf{f})j}$)

$$\Delta\boldsymbol{\psi} = \frac{\Delta\chi_{(\mathbf{f})4} + \Delta\chi_{(\mathbf{f})7}}{2} \mathbf{f}_1 + \frac{\Delta\chi_{(\mathbf{f})3} - \Delta\chi_{(\mathbf{f})9}}{L} \mathbf{f}_2 + \frac{\Delta\chi_{(\mathbf{f})8} - \Delta\chi_{(\mathbf{f})2}}{L} \mathbf{f}_3 \quad (2.49)$$

Introducing the above leads to an intermediate geometric stiffness matrix which is not symmetric [5]. The missing terms to complete the symmetry of the geometric matrix appear when the elastic restoring force in the beam includes geometrically nonlinear effects of bowing of the axis. This bowing introduces a nonlinear relationship between the natural forces and the natural deformations, and couples torsion and moments with the axial and shear forces. This is termed the non-constitutive contributions from deformation modes. The computation of the elastic forces in this work does not include these contributions.

On the other hand, it is possible to amend the intermediate non-symmetric geometric stiffness by introducing rigid body node rotations as shown by Krenk [5]. The resulting symmetric geometric stiffness matrix is consistent with the computation of the elastic forces as described in this report, and because it is consistent with the first order elastic force computation it is called the first-order geometric stiffness.

First-order stiffness.

The four submatrices $K_{(f),AB}^G$ of the geometric stiffness that link nodes $A = I, J$ and $B = I, J$ are given below. Note that these are components on the element frame. The components in the global Cartesian basis may be obtained by the transformation

$$\mathbf{K}^G = \mathbf{T} \mathbf{K}_{(f)}^G \mathbf{T}^T. \quad (2.50)$$

$$K_{(f),II}^G = \begin{bmatrix} 0, & -\frac{S_2}{L}, & -\frac{S_3}{L}, & 0, & 0, & 0 \\ -\frac{S_2}{L}, & N/L, & 0, & -M_{2I}/L, & M_1/L, & 0 \\ -\frac{S_3}{L}, & 0, & N/L, & -M_{3I}/L, & 0, & M_1/L \\ 0, & -M_{2I}/L, & -M_{3I}/L, & 0, & M_{3I}/2, & -M_{2I}/2 \\ 0, & M_1/L, & 0, & M_{3I}/2, & 0, & 0 \\ 0, & 0, & M_1/L, & -M_{2I}/2, & 0, & 0 \end{bmatrix} \quad (2.51)$$

$$K_{(f),IJ}^G = \begin{bmatrix} 0, & -\frac{S_2}{L}, & -\frac{S_3}{L}, & 0, & 0, & 0 \\ -\frac{S_2}{L}, & N/L, & 0, & -M_{2J}/L, & M_1/L, & 0 \\ -\frac{S_3}{L}, & 0, & N/L, & -M_{3J}/L, & 0, & M_1/L \\ 0, & -M_{2J}/L, & -M_{3J}/L, & 0, & -M_{3J}/2, & M_{2J}/2 \\ 0, & M_1/L, & 0, & -M_{3J}/2, & 0, & 0 \\ 0, & 0, & M_1/L, & M_{2J}/2, & 0, & 0 \end{bmatrix} \quad (2.52)$$

$$K_{(f),JI}^G = K_{(f),IJ}^G{}^T \quad (2.53)$$

$$K_{(f),JJ}^G = \begin{bmatrix} 0, & -\frac{S_2}{L}, & -\frac{S_3}{L}, & 0, & 0, & 0 \\ -\frac{S_2}{L}, & N/L, & 0, & -M_{2J}/L, & M_1/L, & 0 \\ -\frac{S_3}{L}, & 0, & N/L, & -M_{3J}/L, & 0, & M_1/L \\ 0, & -M_{2J}/L, & -M_{3J}/L, & 0, & -M_{3J}/2, & M_{2J}/2 \\ 0, & M_1/L, & 0, & -M_{3J}/2, & 0, & 0 \\ 0, & 0, & M_1/L, & M_{2J}/2, & 0, & 0 \end{bmatrix} \quad (2.54)$$

In the above formulae the following symbols are used for convenience:

$$M_{2I} = P_{N4} + P_{N5}, \quad M_{2J} = P_{N4} - P_{N5}$$

and

$$M_{3I} = -(P_{N2} + P_{N3}), \quad M_{3J} = -(P_{N2} - P_{N3})$$

where the natural forces were defined in Section 2.5.

Second-order geometric stiffness.

If the elastic restoring force in the beam included the geometrically nonlinear effects of bowing of the axis, the geometric stiffness matrix would naturally be computed as symmetric [3, 5]. Because it is consistent with the second order elastic force computation it is called the second-order geometric stiffness. Note that the second-order geometric stiffness matrix is inconsistent with the computation of the elastic forces as described in this report. Nevertheless this inconsistency is normally insignificant since it vanishes as the natural deformations become infinitesimally small, and small natural deformations are the intended application area for the present model.

The four submatrices $K_{(f),AB}^G$ of the geometric stiffness that link nodes $A = I, J$ and $B = I, J$ are given below. Note that these are components on the element frame.

$$K_{(f),II}^G = \begin{bmatrix} 0, & -\frac{S_2}{L}, & -\frac{S_3}{L}, & 0, & 0, & 0 \\ -\frac{S_2}{L}, & \frac{6N}{5L}, & 0, & \frac{S_3}{2} - \frac{M_{2s}}{L}, & M_1/L, & N/10 \\ -\frac{S_3}{L}, & 0, & \frac{6N}{5L}, & -\frac{S_2}{2} - \frac{M_{3s}}{L}, & -N/10, & M_1/L \\ 0, & \frac{S_3}{2} - \frac{M_{2s}}{L}, & -\frac{S_2}{2} - \frac{M_{3s}}{L}, & \frac{N(I_2 + I_3)}{AL}, & \frac{M_{3s}}{2} + \frac{LS_2}{12}, & \frac{LS_3}{12} - \frac{M_{2s}}{2} \\ 0, & M_1/L, & -N/10, & \frac{M_{3s}}{2} + \frac{LS_2}{12}, & (2LN)/15, & 0 \\ 0, & N/10, & M_1/L, & \frac{LS_3}{12} - \frac{M_{2s}}{2}, & 0, & (2LN)/15 \end{bmatrix} \quad (2.55)$$

$$K_{(f),IJ}^G = \begin{bmatrix} 0, & \frac{S_2}{L}, & \frac{S_3}{L}, & 0, & 0, & 0 \\ \frac{S_2}{L}, & -\frac{6N}{5L}, & 0, & \frac{S_3}{2} + \frac{M_{2s}}{L}, & -M_1/L, & N/10 \\ \frac{S_3}{L}, & 0, & -\frac{6N}{5L}, & \frac{M_{3s}}{L} - \frac{S_2}{2}, & -N/10, & -M_1/L \\ 0, & \frac{M_{2s}}{L} - \frac{S_3}{2}, & \frac{S_2}{2} + \frac{M_{3s}}{L}, & -\frac{N(I_2 + I_3)}{AL}, & (LS_2)/6, & (LS_3)/6 \\ 0, & -M_1/L, & N/10, & (LS_2)/6, & -(LN)/30, & M_1/2 \\ 0, & -N/10, & -M_1/L, & (LS_3)/6, & -M_1/2, & -(LN)/30 \end{bmatrix} \quad (2.56)$$

$$K_{(f),JI}^G = K_{(f),IJ}^{G^T} \quad (2.57)$$

$$K_{(f),JJ}^G = \begin{bmatrix} 0, & -\frac{S_2}{L}, & -\frac{S_3}{L}, & 0, & 0, & 0 \\ -\frac{S_2}{L}, & \frac{6N}{5L}, & 0, & -\frac{S_3}{2} - \frac{M_{2s}}{L}, & M_1/L, & -N/10 \\ -\frac{S_3}{L}, & 0, & \frac{6N}{5L}, & \frac{S_2}{2} - \frac{M_{3s}}{L}, & N/10, & M_1/L \\ 0, & -\frac{S_3}{2} - \frac{M_{2s}}{L}, & \frac{S_2}{2} - \frac{M_{3s}}{L}, & \frac{N(I_2 + I_3)}{AL}, & \frac{LS_2}{12} - \frac{M_{3s}}{2}, & \frac{M_{2s}}{2} + \frac{LS_3}{12} \\ 0, & M_1/L, & N/10, & \frac{LS_2}{12} - \frac{M_{3s}}{2}, & (2LN)/15, & 0 \\ 0, & -N/10, & M_1/L, & \frac{M_{2s}}{2} + \frac{LS_3}{12}, & 0, & (2LN)/15 \end{bmatrix} \quad (2.58)$$

In the above formulae the following symbols are used for convenience:

$$M_{2s} = P_{N4}, \quad M_{3s} = -P_{N2}$$

where the natural forces were defined in Section 2.5.

2.10.3 Load-dependent stiffness matrix

As shown by Argyris [2, 3] the manner in which conservative external moments are applied to the structure matters in stability analyses. Incremental rotations of the nodes to which conservative external moments are applied may or may not generate a load-dependent stiffness matrix. It is shown in References [2, 3], and later elaborated by Krysl [6] for the present representation of finite rotations, that axial and semi-tangential external moments do not generate additional load-dependent stiffness matrices; on the other hand, quasi-tangential external moments do generate a load-dependent stiffness matrix.

For the quasi-tangential moment acting at node J we define the unit vectors \mathbf{k} and ℓ in the direction of the torque-generating force and the lever respectively (refer to Figure 2.8). The magnitude of the applied moment is given as $\|\mathbf{M}^{(J)}\|$, and its direction is $\ell \times \mathbf{k}$. The load-dependent stiffness to be assembled to the degrees of freedom corresponding to rotations and moments at node J reads

$$\mathbf{K}^L = \frac{\|\mathbf{M}^{(J)}\|}{2} (\ell \mathbf{k}^T + \mathbf{k} \ell^T) \quad (2.59)$$

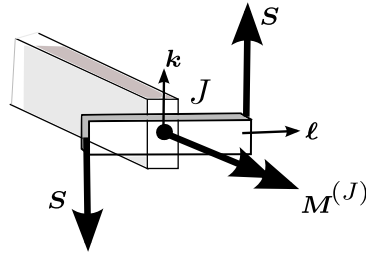


Fig. 2.8. Schematic of an external moment applied quasi-tangentially at node J .

2.11 Mass matrix and gyroscopic matrix

The kinetic energy may be written for a single beam as

$$K = \frac{1}{2} \mathbf{v}^T \mathbf{M} \mathbf{v} , \quad (2.60)$$

where \mathbf{M} is the element mass matrix, and \mathbf{v} is the vector of translational and rotational velocities of the two nodes.

The contribution of the kinetic energy to the equations of motion (the Euler-Lagrange equations) is

$$\frac{d}{dt} \frac{\partial K}{\partial \mathbf{v}} = \frac{d}{dt} \mathbf{v}^T \mathbf{M} . \quad (2.61)$$

In the corotational framework the mass matrix is expressed as a transformation of the constant mass matrix in the element frame $\mathbf{M}_{(f)}$

$$\mathbf{M} = \mathbf{T} \mathbf{M}_{(f)} \mathbf{T}^T . \quad (2.62)$$

Importantly, the transformation (rotation) matrix \mathbf{T} changes with time because of the change of the configuration. Therefore, upon substitution of (2.62) into (2.61) leads to

$$\frac{d}{dt} \mathbf{v}^T \mathbf{M} = \dot{\mathbf{v}}^T \mathbf{M} + \mathbf{v}^T \dot{\mathbf{M}} = \dot{\mathbf{v}}^T \mathbf{M} + \mathbf{v}^T \left(\dot{\mathbf{T}} \mathbf{M}_{(f)} \mathbf{T}^T + \mathbf{T} \mathbf{M}_{(f)} \dot{\mathbf{T}}^T \right) \quad (2.63)$$

The time derivative of the elementwise transformation matrix introduced in (2.23) is obtained by expressing the time derivative of the element frame (2.7)

$${}^t \dot{\mathbf{F}} = \left[{}^t \dot{\mathbf{f}}_1, {}^t \dot{\mathbf{f}}_2, {}^t \dot{\mathbf{f}}_3 \right] . \quad (2.64)$$

Given that the frame basis vectors are an orthogonal set, their time derivatives may be expressed as

$${}^t \dot{\mathbf{f}}_k = \boldsymbol{\omega} \times {}^t \mathbf{f}_k , \quad (2.65)$$

where $\boldsymbol{\omega}$ is the angular velocity of the element frame. Using the equivalent expression of the cross product as a multiplication with a skew-symmetric matrix

$$\boldsymbol{\omega} \times {}^t \mathbf{f}_k = \tilde{\boldsymbol{\omega}} \cdot {}^t \mathbf{f}_k \quad (2.66)$$

where $\tilde{\boldsymbol{\omega}}$ indicates the skew symmetric matrix associated with the axial vector $\boldsymbol{\omega}$, we can write

$${}^t \dot{\mathbf{F}} = \tilde{\boldsymbol{\omega}} \cdot {}^t \mathbf{F} \quad (2.67)$$

Therefore, introducing the matrix

$$\tilde{\boldsymbol{\Omega}} = \begin{bmatrix} \tilde{\boldsymbol{\omega}} & \mathbf{0} & \mathbf{0} & \mathbf{0} \\ \mathbf{0} & \tilde{\boldsymbol{\omega}} & \mathbf{0} & \mathbf{0} \\ \mathbf{0} & \mathbf{0} & \tilde{\boldsymbol{\omega}} & \mathbf{0} \\ \mathbf{0} & \mathbf{0} & \mathbf{0} & \tilde{\boldsymbol{\omega}} \end{bmatrix} \quad (2.68)$$

we may write

$$\dot{\mathbf{T}} = \tilde{\boldsymbol{\Omega}} \cdot \mathbf{T} . \quad (2.69)$$

Consequently, equation (2.63) may be rewritten

$$\frac{d}{dt} \mathbf{v}^T \mathbf{M} = \dot{\mathbf{v}}^T \mathbf{M} + \mathbf{v}^T \left(\tilde{\boldsymbol{\Omega}} \cdot \mathbf{T} \mathbf{M}_{(f)} \mathbf{T}^T + \mathbf{T} \mathbf{M}_{(f)} \left(\tilde{\boldsymbol{\Omega}} \cdot \mathbf{T} \right)^T \right) \quad (2.70)$$

or

$$\frac{d}{dt} \mathbf{v}^T \mathbf{M} = \dot{\mathbf{v}}^T \mathbf{M} + \mathbf{v}^T \left(\tilde{\boldsymbol{\Omega}} \cdot \mathbf{M} + \mathbf{M} \cdot \tilde{\boldsymbol{\Omega}}^T \right) \quad (2.71)$$

The first term on the right is the expected mass matrix of the element in the global Cartesian coordinates

$$\mathbf{M} = \mathbf{T} \mathbf{M}_{(f)} \mathbf{T}^T \quad (2.72)$$

which contributes the inertial force

$$\mathbf{M} \dot{\mathbf{v}} = \mathbf{M} \mathbf{a}, \quad (2.73)$$

where \mathbf{a} is the vector of nodal accelerations.

The second term on the right of (2.71) defines the matrix \mathbf{G} that produces the gyroscopic force

$$\mathbf{G} = \tilde{\boldsymbol{\Omega}} \cdot \mathbf{M} + \mathbf{M} \cdot \tilde{\boldsymbol{\Omega}}^T \quad (2.74)$$

as $\mathbf{G} \mathbf{v}$. The matrix \mathbf{G} is commonly denoted as the gyroscopic matrix. It is interesting to note that in the present formulation the gyroscopic matrix is symmetric which is in stark contrast to the usual skew-symmetric form of this matrix commonly found in the literature.

The element frame angular velocity may be computed by an obvious modification of the incremental rotation vector (2.49)

$$\boldsymbol{\omega} = \frac{v_{(f)4} + v_{(f)7}}{2} \mathbf{f}_1 + \frac{v_{(f)3} - v_{(f)9}}{L} \mathbf{f}_2 + \frac{v_{(f)8} - v_{(f)2}}{L} \mathbf{f}_3, \quad (2.75)$$

and consists of axial angular velocity (first term), and transverse angular velocity (second and third term).

2.11.1 Consistent mass matrix

The consistent mass matrix of the beam element in the element frame may be composed of two parts. The first part takes into consideration only inertia due to translation of the nodes and rotation about the beam's axis; the second part includes the effect of the rotation of the nodes about the x_2 and x_3 element-frame axes.

The first part can be detailed as the four submatrices ${}^1M_{(f),AB}$ that link nodes $A = I, J$ and $B = I, J$:

$${}^1M_{(f),II} = AL\rho \begin{bmatrix} 1/3, & 0, & 0, & 0, & 0, & 0 \\ 0, & 13/35, & 0, & 0, & 0, & (11L)/210 \\ 0, & 0, & 13/35, & 0, & -(11L)/210, & 0 \\ 0, & 0, & 0, & I_1/(3A), & 0, & 0 \\ 0, & 0, & -(11L)/210, & 0, & L^2/105, & 0 \\ 0, & (11L)/210, & 0, & 0, & 0, & L^2/105 \end{bmatrix} \quad (2.76)$$

$${}^1M_{(f),IJ} = AL\rho \begin{bmatrix} 1/6, & 0, & 0, & 0, & 0, & 0 \\ 0, & 9/70, & 0, & 0, & 0, & -(13L)/420 \\ 0, & 0, & 9/70, & 0, & (13L)/420, & 0 \\ 0, & 0, & 0, & I_1/(6A), & 0, & 0 \\ 0, & 0, & -(13L)/420, & 0, & -L^2/140, & 0 \\ 0, & (13L)/420, & 0, & 0, & 0, & -L^2/140 \end{bmatrix} \quad (2.77)$$

$${}^1M_{(\mathbf{f}),JI} = {}^1M_{(\mathbf{f}),IJ} \quad (2.78)$$

$${}^1M_{(\mathbf{f}),JJ} = AL\rho \begin{bmatrix} 1/3, & 0, & 0, & 0, & 0, & 0 \\ 0, & 13/35, & 0, & 0, & 0, & -(11L)/210 \\ 0, & 0, & 13/35, & 0, & (11L)/210, & 0 \\ 0, & 0, & 0, & I_1/(3A), & 0, & 0 \\ 0, & 0, & (11L)/210, & 0, & L^2/105, & 0 \\ 0, & -(11L)/210, & 0, & 0, & 0, & L^2/105 \end{bmatrix} \quad (2.79)$$

The second part, which adds the transverse rotations, are the four submatrices ${}^2M_{(\mathbf{f}),AB}$ that link nodes $A = I, J$ and $B = I, J$ as

$${}^2M_{(\mathbf{f}),II} = \rho/L \begin{bmatrix} 0, & 0, & 0, & 0, & 0, & 0 \\ 0, & (6I_2)/5, & 0, & 0, & 0, & (I_2L)/10 \\ 0, & 0, & (6I_3)/5, & 0, & -(I_3L)/10, & 0 \\ 0, & 0, & 0, & 0, & 0, & 0 \\ 0, & 0, & -(I_3L)/10, & 0, & (2I_3L^2)/15, & 0 \\ 0, & (I_2L)/10, & 0, & 0, & 0, & (2I_2L^2)/15 \end{bmatrix} \quad (2.80)$$

$${}^2M_{(\mathbf{f}),IJ} = \rho/L \begin{bmatrix} 0, & 0, & 0, & 0, & 0, & 0 \\ 0, & -(6I_2)/5, & 0, & 0, & 0, & (I_2L)/10 \\ 0, & 0, & -(6I_3)/5, & 0, & -(I_3L)/10, & 0 \\ 0, & 0, & 0, & 0, & 0, & 0 \\ 0, & 0, & (I_3L)/10, & 0, & -(I_3L^2)/30, & 0 \\ 0, & -(I_2L)/10, & 0, & 0, & 0, & -(I_2L^2)/30 \end{bmatrix} \quad (2.81)$$

$${}^2M_{(\mathbf{f}),JI} = {}^2M_{(\mathbf{f}),IJ} \quad (2.82)$$

$${}^2M_{(\mathbf{f}),JJ} = \rho/L \begin{bmatrix} 0, & 0, & 0, & 0, & 0, & 0 \\ 0, & (6I_2)/5, & 0, & 0, & 0, & -(I_2L)/10 \\ 0, & 0, & (6I_3)/5, & 0, & (I_3L)/10, & 0 \\ 0, & 0, & 0, & 0, & 0, & 0 \\ 0, & 0, & (I_3L)/10, & 0, & (2I_3L^2)/15, & 0 \\ 0, & -(I_2L)/10, & 0, & 0, & 0, & (2I_2L^2)/15 \end{bmatrix} \quad (2.83)$$

2.11.2 Lumped mass matrix

The lumped (diagonal) mass matrix of the beam element in the element frame may be formulated by assigning part of the beam total inertia to the diagonal elements of the mass matrix.

The simplest lumped mass matrix takes into consideration only inertia due to translation of the nodes:

$${}^iM_{(f)} = (AL\rho/2) \begin{bmatrix} 1, 0, 0, 0, 0, 0, 0, 0, 0, 0, 0, 0 \\ 0, 1, 0, 0, 0, 0, 0, 0, 0, 0, 0, 0 \\ 0, 0, 1, 0, 0, 0, 0, 0, 0, 0, 0, 0 \\ 0, 0, 0, 0, 0, 0, 0, 0, 0, 0, 0, 0 \\ 0, 0, 0, 0, 0, 0, 0, 0, 0, 0, 0, 0 \\ 0, 0, 0, 0, 0, 0, 0, 0, 0, 0, 0, 0 \\ 0, 0, 0, 0, 0, 0, 0, 0, 0, 0, 0, 0 \\ 0, 0, 0, 0, 0, 0, 1, 0, 0, 0, 0, 0 \\ 0, 0, 0, 0, 0, 0, 0, 1, 0, 0, 0, 0 \\ 0, 0, 0, 0, 0, 0, 0, 0, 1, 0, 0, 0 \\ 0, 0, 0, 0, 0, 0, 0, 0, 0, 1, 0, 0 \\ 0, 0, 0, 0, 0, 0, 0, 0, 0, 0, 1, 0 \end{bmatrix} \quad (2.84)$$

The below lumped mass matrix also includes mass moments of inertia assigned to the rotational degrees of freedom.

$${}^dM_{(f),IJ} = (AL\rho/2) \begin{bmatrix} 1, 0, 0, 0, 0, 0, 0, 0, 0, 0, 0, 0 \\ 0, 1, 0, 0, 0, 0, 0, 0, 0, 0, 0, 0 \\ 0, 0, 1, 0, 0, 0, 0, 0, 0, 0, 0, 0 \\ 0, 0, 0, I_1/A, 0, 0, 0, 0, 0, 0, 0, 0 \\ 0, 0, 0, 0, I_2/A, 0, 0, 0, 0, 0, 0, 0 \\ 0, 0, 0, 0, 0, I_3/A, 0, 0, 0, 0, 0, 0 \\ 0, 0, 0, 0, 0, 0, 1, 0, 0, 0, 0, 0 \\ 0, 0, 0, 0, 0, 0, 0, 1, 0, 0, 0, 0 \\ 0, 0, 0, 0, 0, 0, 0, 0, 1, 0, 0, 0 \\ 0, 0, 0, 0, 0, 0, 0, 0, 0, 1, 0, 0 \\ 0, 0, 0, 0, 0, 0, 0, 0, 0, 0, I_1/A \\ 0, 0, 0, 0, 0, 0, 0, 0, 0, 0, I_2/A, 0 \\ 0, 0, 0, 0, 0, 0, 0, 0, 0, 0, 0, I_3/A \end{bmatrix} \quad (2.85)$$

$${}^1M_{(f),JI} = {}^1M_{(f),IJ} \quad (2.86)$$

$${}^1M_{(f),JJ} = AL\rho \begin{bmatrix} 1/3, & 0, & 0, & 0, & 0, & 0 \\ 0, & 13/35, & 0, & 0, & 0, & -(11L)/210 \\ 0, & 0, & 13/35, & 0, & (11L)/210, & 0 \\ 0, & 0, & 0, & I_1/(3A), & 0, & 0 \\ 0, & 0, & (11L)/210, & 0, & L^2/105, & 0 \\ 0, & -(11L)/210, & 0, & 0, & 0, & L^2/105 \end{bmatrix} \quad (2.87)$$

2.12 Damping matrix

The Rayleigh proportional damping matrix is a linear combination of the elastic stiffness and the mass matrix

$$\mathbf{C} = \alpha \mathbf{M} + \beta \mathbf{K}^E. \quad (2.88)$$

The coefficients of the linear combination may be determined from given damping ratios ζ_1 and ζ_2 for two distinct natural frequencies ω_1 and ω_2

$$\alpha = \frac{2[\omega_1\omega_2^2\zeta_1 - \omega_1^2\omega_2\zeta_2]}{(\omega_2^2 - \omega_1^2)}, \quad \beta = \frac{2[-\omega_1\zeta_1 + \omega_2\zeta_2]}{(\omega_2^2 - \omega_1^2)}. \quad (2.89)$$

2.13 Modal analysis

Consider the system of interconnected beams (i.e. the structure) in some configuration ${}^n\chi$. The equation of small-amplitude perturbation motion superimposed on the known configuration ${}^n\chi$ may be written as

$$\mathbf{M}\ddot{\Delta\chi} + \mathbf{C}\dot{\Delta\chi} + \mathbf{K}\Delta\chi = \Delta\mathbf{L}, \quad (2.90)$$

All matrices depend on the current configuration ${}^n\chi$. It was assumed that the loading on the right-hand side does not change with the vibration. The tangent stiffness \mathbf{K} will include both elastic and geometric effects, and the damping matrix \mathbf{C} could include gyroscopic effects. The perturbation load $\Delta\mathbf{L}$ may or may not be zero.

If the perturbation load is indeed $\Delta\mathbf{L}$ identically zero, we have the case of free vibration: Assuming that the small-amplitude superimposed vibration is harmonic

$$\Delta\chi = \exp \lambda t \phi, \quad (2.91)$$

where λ is complex, and ϕ is a time-independent vector, we can write the quadratic eigenvalue problem

$$\lambda^2 \mathbf{M}\phi + \lambda \mathbf{C}\phi + \mathbf{K}\phi = \mathbf{0}. \quad (2.92)$$

The quadratic eigenvalue problem may be solved by converting the equations of motion to first order form and then solving an eigenvalue problem in standard form but of double size.

If for the purpose of investigating the small-amplitude vibration we can neglect the velocity dependent terms (material damping and gyroscopic effects), the quadratic eigenvalue problem (2.92) reduces to the well-known free-vibration equation

$$\lambda^2 \mathbf{M}\phi + \mathbf{K}\phi = \mathbf{0}, \quad (2.93)$$

or, with the natural frequency $\omega = i\lambda$

$$-\omega^2 \mathbf{M}\phi + \mathbf{K}\phi = \mathbf{0} . \quad (2.94)$$

Both the mass matrix and the tangent stiffness matrix are symmetric, and if the stiffness matrix is also positive definite (i.e. the structure is in a stable equilibrium) the natural frequencies are all positive and real, $\omega \geq 0$. If the structure is free-floating, or in neutral equilibrium (such as occurs at bifurcation) the stiffness matrix may be positive semi-definite, and some natural frequencies may become zero. If the structure has passed through a bifurcation point and is in a state of unstable equilibrium, the stiffness matrix is indefinite and some natural frequencies become imaginary ($\omega^2 \leq 0$).

2.14 Buckling analysis

For static deformation the equation of motion is the equation of static equilibrium (2.26). For the case of external loads which are expressed as a function of a single load parameter λ we have

$$\mathbf{L}(\lambda) + \mathbf{r}(\chi(\lambda)) = \mathbf{0} \quad (2.95)$$

The set of solutions of static equilibrium as the load parameter varies describes a curve in the configuration parameter space. Some equilibrium points may be associated with buckling (bifurcation) where two or more equilibrium curves branch out. Other equilibrium points may be associated with maximum or minimum in the load-displacement curve – the limit points [6].

For static deformation equation (2.90) for small-amplitude perturbation from an equilibrium configuration ${}^n\chi$ reduces to

$$\mathbf{K}\Delta\chi = \Delta\mathbf{L} . \quad (2.96)$$

When the attained configuration is associated with a bifurcation (buckling) or limit state, that is with neutral equilibrium, equation (2.96) will have a nonzero solution for the perturbation displacement even for no change in the applied load:

$$\mathbf{K}\Delta\chi = \mathbf{0} . \quad (2.97)$$

which simply states that tangent stiffness matrix of the structure is singular.

If the applied load depends on a single load parameter

$$\mathbf{L}(\lambda) = \lambda \bar{\mathbf{L}} , \quad (2.98)$$

where $\bar{\mathbf{L}}$ is a constant vector that describes the distribution of the load over the structure, we can write the perturbation load as

$$\Delta\mathbf{L}(\lambda) = \Delta\lambda \bar{\mathbf{L}} , \quad (2.99)$$

and the tangent stiffness as

$$\mathbf{K}(\lambda) = \mathbf{K}^E(\lambda) + \mathbf{K}^G(\lambda) + \mathbf{K}^L(\lambda) . \quad (2.100)$$

Let us assume that for a given load parameter ${}^n\lambda$ the structure assumed the configuration ${}^n\chi$. The critical value of the load parameter at which the structure enters neutral equilibrium (buckling or limit point) may be estimated from the condition that at the critical load parameter λ_{cr} we have

$$\mathbf{K}(\lambda_{\text{cr}})\Delta\chi = \mathbf{0} , \quad (2.101)$$

where we may express

$$\mathbf{K}(\lambda_{\text{cr}}) = \mathbf{K}({}^n\lambda) + \frac{\partial \mathbf{K}({}^n\lambda)}{\partial \lambda}(\lambda_{\text{cr}} - {}^n\lambda) \quad (2.102)$$

Therefore we have the eigenvalue problem

$$\mathbf{K}({}^n\lambda)\Delta\chi = -(\lambda_{\text{cr}} - {}^n\lambda)\frac{\partial\mathbf{K}({}^n\lambda)}{\partial\lambda}\Delta\chi. \quad (2.103)$$

The derivative of the tangent stiffness may be estimated using divided differences

$$\frac{\partial\mathbf{K}({}^n\lambda)}{\partial\lambda}({}^{n+1}\lambda - {}^n\lambda) \approx \mathbf{K}({}^{n+1}\lambda) - \mathbf{K}({}^n\lambda) \quad (2.104)$$

as the difference of the tangent stiffnesses in two different configurations, for the load parameters ${}^{n+1}\lambda$ and ${}^n\lambda$.

For instance, take $n = 0$. Then the configuration ${}^n\chi = {}^0\chi$ is the stress free initial configuration (there is no load, ${}^0\lambda = 0$). Furthermore take ${}^{n+1}\lambda = 1$. Then we have

$$\mathbf{K}(0) = \mathbf{K}^E(0), \quad (2.105)$$

and

$$\mathbf{K}(1) = \mathbf{K}^E(1) + \mathbf{K}^G(1) + \mathbf{K}^L(1), \quad (2.106)$$

If we also assume that the elastic stiffness does not change $\mathbf{K}^E(1) = \mathbf{K}^E(0)$ we obtain the so-called linear buckling problem

$$\mathbf{K}^E(0)\Delta\chi = -\lambda_{\text{cr}}\left(\mathbf{K}^G(1) + \mathbf{K}^L(1)\right)\Delta\chi. \quad (2.107)$$

2.15 Frictionless contact

The derivations in this section are applicable to beams with *circular cross section*. We consider a borehole of circular cross-section of radius r_B with center at C_B . The drill string of external radius r_E is located inside the borehole with center at C_E (call for Figure 2.9). The frictionless contact of the drill string with the borehole is enforced with a penalty method, which is implemented with a mechanical element called the *tieline*.

The tieline t is a nonlinear spring which connects the center of the borehole with the center of the drill string. The functional relationship for the force transmitted by the tieline is formulated so that the force is negligible until the drill string circumference enters the circle of radius r_c . The force in the tieline then sharply increases and when the drill string circumference touches the circle of radius r_B (i.e. the borehole surface) the tieline force attains a given value to which the contact force is calibrated (the maximum likely contact force F_1). The ratio $(r_B - r_c)/r_B$ is an input parameter called *contact layer fraction*. Another way of thinking of the contact enforcement is to imagine that the tieline constrains the center of the drill string to move only within a circle at C_B of radius $r_t = r_B - r_E$ (r_t is called the tieline distance).

2.15.1 Formulation of tieline force

The total weight of the drill string may be used as an estimate of the largest likely contact force F_1 , especially for almost vertical drill strings.

The functional relationship between the distance d of the node at the center C_E of the drill string segment and the center of the borehole and the tieline force F is taken here as (refer to Figure 2.10)

$$F(d) = \begin{cases} \left(\frac{d}{r_t}\right)^p F_1, & \text{if } d < r_t; \\ F_1 + pF_1\left(\frac{d}{r_t} - 1\right), & \text{otherwise.} \end{cases} \quad (2.108)$$

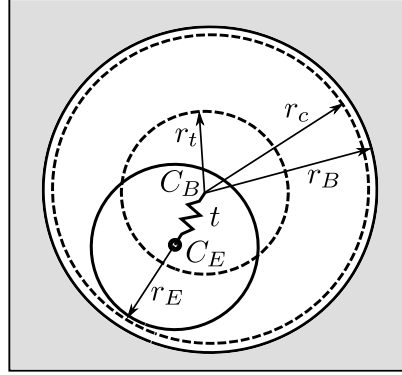


Fig. 2.9. The tieline mechanical element to enforce contact of the drill string with the borehole

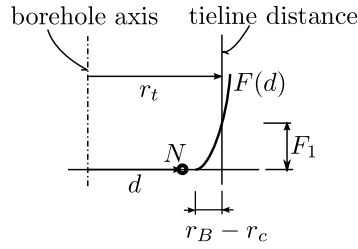


Fig. 2.10. Relationship of the distance of the drill string center from the center of the borehole and the contact force

The exponent p in (2.108) is computed from the condition that the force should increase from negligible to F_1 within the given thickness of the contact layer $r_B - r_c$. We take the negligible contact force κF_1 to be a small fraction of F_1 , $\kappa \ll 1$, and use (2.108) to compute the exponent

$$p = \frac{\ln \kappa}{\ln \frac{r_t - (r_B - r_c)}{r_t}}$$

2.15.2 Frictional contact

The drill string may be in contact with the borehole which may affect its torsional and axial frequencies of forced vibration. In direct time integration procedures the Coulomb model of frictional damping may be effective.

Figure 2.11 shows a schematic of a drillstring in contact with the borehole. The normal contact force \mathbf{N} points from the contact point C towards the center of the drillstring C_E , the frictional force \mathbf{F} opposes the sliding along the borehole wall which is given by the direction of the spin of the drill string ω . The magnitude of the frictional force may be taken as a variation on the basic Coulomb model

$$\|\mathbf{F}\| = \mu \|\mathbf{N}\|$$

where μ is the coefficient of friction. Assuming that the drill string is spinning is about a tangent to the centerline of the borehole \mathbf{e}_1 such that its angular velocity is

$$\boldsymbol{\omega} = \omega \mathbf{e}_1$$

the frictional torque \mathbf{T} about the center of the drill string C_E is

$$\mathbf{T} = -\text{sign}(\omega) \mu \|\mathbf{N}\| r_E \mathbf{e}_1 .$$

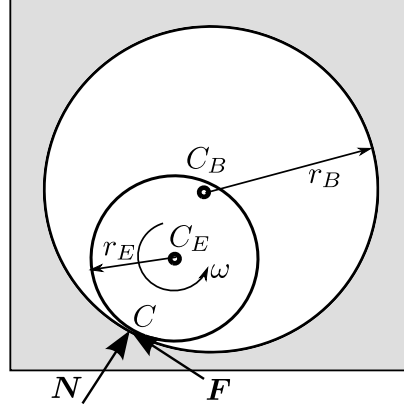


Fig. 2.11. The frictional contact of the drill string with the borehole

In forced-vibration analysis in which the drill string undergoes torsional oscillations the effect of the frictional contact may be incorporated in a simplified way using an equivalent viscous damping model. Equating the energy dissipated by friction damping and the energy dissipated by the equivalent viscous mechanism we can formulate the equivalent damping coefficient as [11]

$$C_{equiv} = \frac{4\mu\|N\|}{\pi|\omega|} \quad (2.109)$$

where $|\omega|$ is the magnitude of the angular velocity of the equivalent motion.

2.16 Drilling fluid effects

The drilling mud is assumed for this purpose to be a Newtonian fluid, with constant dynamic viscosity. The transverse motion of the beam generates an in-phase force (inertial) which is represented by an added mass matrix, and out of phase force (damping) which is represented by fluid-drag matrix. The treatment below is based on the theoretical study of Wambsganss et al. [13]. The derivations are applicable to beams with *circular cross section*, contained in a concentric borehole with circular cross-section. The end-flow effects are ignored in the formulation.

In the following we shall assume that the borehole is of circular cross-section of radius r_B , and the vibrating beam is of solid circular cross-section of radius r_E . Note that if the beam is hollow, such as a pipe, the effect of the exterior fluid is not affected by the presence of the void inside the beam. The material (drilling mud) inside the pipe is accounted for by adding the mass of the fluid inside to the mass matrix. The damping of transverse vibrations by the internal viscous fluid is usually neglected, and it will be neglected here too. In this formulation the rotation of the beam or its axial motion in the fluid does not contribute to the added mass or to damping mechanisms.

The mass of the fluid displaced by the transversely vibrating beam per unit length is

$$M_f = \rho_f \pi r_E^2 \quad (2.110)$$

where ρ_f is the mass density of the fluid.

2.16.1 Added mass matrix

The added mass per unit length is

$$M_a = \text{Re}H(S)M_f$$

where M_f is the mass of the displaced fluid from (2.110), $H(S)$ is a function to be described next, and S is the Stokes number

$$S(\omega, r_E, \nu_f) = \frac{\omega r_E^2}{\nu_f} \quad (2.111)$$

where ω is the angular frequency of the motion, and ν_f is the kinematic viscosity of the fluid. For angular frequency corresponding to 100 rpm motion ($\omega = 10.47$ rad/s) and radius $r_E = 0.1$ m the Stokes number is $S \approx 104700$ for water (mass density $\rho_f = 1000$ kg/m³, dynamic viscosity $\mu_f \approx 1.0$ cP = 0.001 kg/m/s), and $S \approx 5240$ for relatively viscous drilling mud (mass density $\rho_f = 1500$ kg/m³, dynamic viscosity $\mu_f \approx 30.0$ cP = 0.03 kg/m/s).

The complex-valued function $H(S)$ was obtained in Reference [13] in terms of two dimensionless variables

$$\alpha = \sqrt{i \frac{\omega}{\nu_f}} r_E, \quad \beta = \sqrt{i \frac{\omega}{\nu_f}} r_B$$

Given that $|\alpha| > \sqrt{S}$ and $|\beta| > |\alpha|$, the approximation of H for large absolute values of the coefficients α and β can be adopted

$$H = \frac{[\alpha^2(1 + \gamma^2) - 8\gamma] \sinh(\beta - \alpha) + 2\alpha(2 - \gamma + \gamma^2) \cosh(\beta - \alpha) - 2\gamma^2 \sqrt{\alpha\beta} - 2\alpha \sqrt{\alpha/\beta}}{\alpha^2(1 - \gamma^2) \sinh(\beta - \alpha) - 2\alpha\gamma(1 + \gamma) \cosh(\beta - \alpha) + 2\gamma^2 \sqrt{\alpha\beta} + 2\alpha \sqrt{\alpha/\beta}} \quad (2.112)$$

where we have introduced $\gamma = r_E/r_B$ for convenience. The real part $\text{Re}H$ is shown in Figure 2.12.

We use diagonal added mass representation. The lumped mass

$$M = \frac{1}{2} M_a^0 L$$

is added to the degrees of freedom that correspond to the transverse translation of the beam.

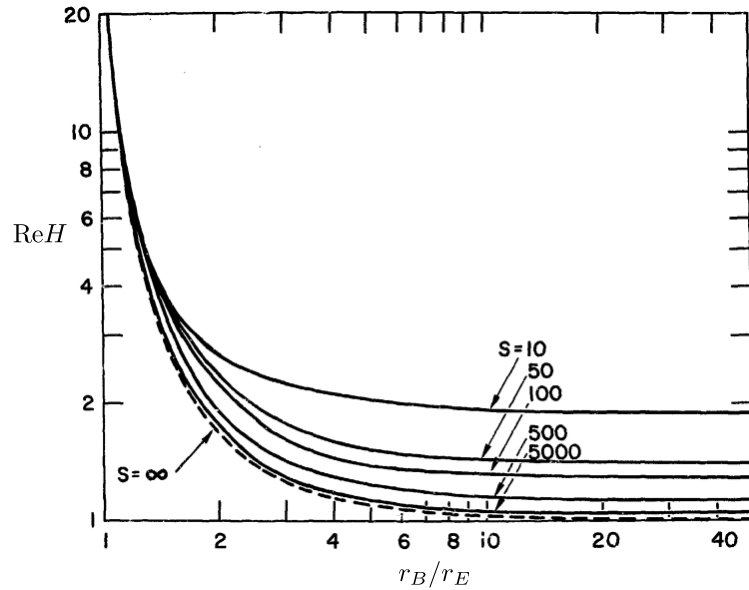


Fig. 2.12. The real part of the function H of (2.112)

2.16.2 Fluid-drag damping matrix

The damping coefficient per unit length is obtained

$$C_a = \omega |\text{Im}H(S)| M_f$$

where M_f is the mass of the displaced fluid from (2.110), $\text{Im}H$ is the imaginary part of the function (2.112), and ω is the angular frequency of the motion. The absolute value of the imaginary part $|\text{Im}H|$ is shown in Figure 2.13.

We use diagonal fluid-drag damping matrix representation. The lumped damping coefficient

$$C = \frac{1}{2} C_a^0 L$$

is added to the degrees of freedom that correspond to the transverse translation of the beam.

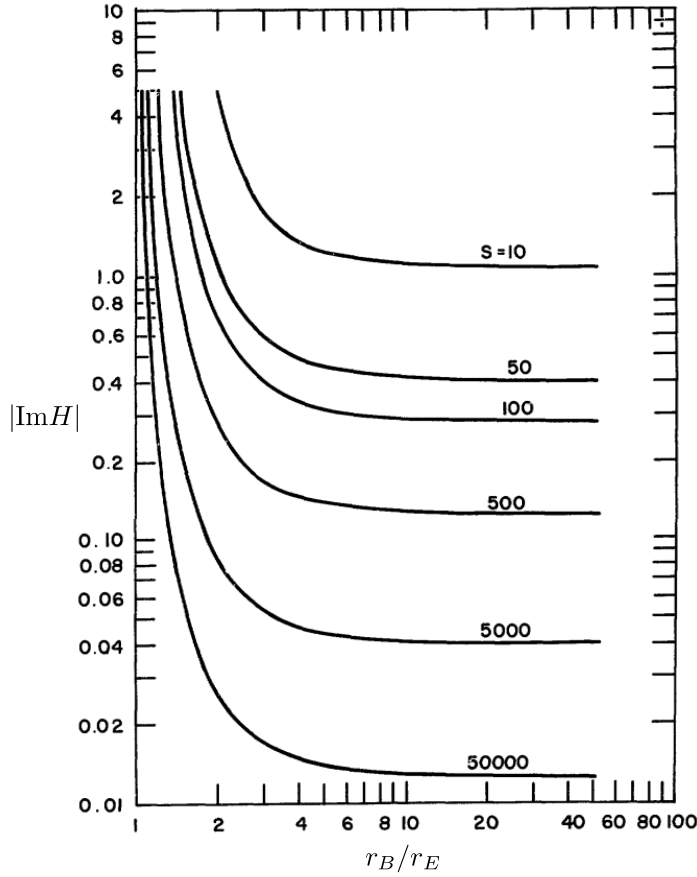


Fig. 2.13. The imaginary part of the function H of (2.112)

2.17 Steady-state motion

When the drillstring moves in steady-state oscillations, the equations of motion may be written as in (2.90). Assuming the steady-state response in the form

$$\Delta \chi = \exp(i\omega t) \phi, \quad (2.113)$$

where ω is the frequency of the applied harmonic load, and ϕ is the (complex) mode vector, the equations of harmonic response may be written as

$$-\omega^2 \mathbf{M} \phi + i\omega \mathbf{C} \phi + \mathbf{K} \phi = \ell . \quad (2.114)$$

Here ℓ is the time-independent distribution of the loads on the structure. For instance, for structure spinning with a given eccentricity about an axis parallel to the midline the loading would correspond to the centrifugal force.

Equation (2.114) may be rewritten as

$$(-\omega^2 \mathbf{M} + i\omega \mathbf{C} + \mathbf{K}) \phi = \ell , \quad (2.115)$$

where the dynamic matrix $-\omega^2 \mathbf{M} + i\omega \mathbf{C} + \mathbf{K}$ is seen to depend on the excitation frequency. The dynamic matrix would typically incorporate several mechanical elements. The mass matrix would consist of the inertial contribution of the drillstring itself, and possibly also of the added mass of the drilling fluid. The damping matrix would incorporate the gyroscopic effects, the fluid-drag effects of the drilling fluid, and the damping inherent to the drillstring itself. The stiffness matrix would include the elastic and geometric stiffness of the structure, which means that any nonzero resultant forces would stiffen or soften the structure.

2.17.1 Critical RPM

The amplitude of the resulting motion may be computed by inverting the dynamic matrix

$$\|\phi\| = \| (-\omega^2 \mathbf{M} + i\omega \mathbf{C} + \mathbf{K})^{-1} \ell \| , \quad (2.116)$$

where the dependence on the excitation frequency should be noted. The diagram of the amplitude of the resulting motion vs. the frequency of excitation provides insight into the behavior of the structure at various frequencies, and it is computed by sweeping across the frequencies and solving repeatedly equation (2.116). Peaks of the resulting motion in the diagram occur at the so-called critical frequencies (critical RPMs).

Verification

3.1 Linear buckling

The verification examples in this section obtain the critical buckling loads by solving (2.107).

3.1.1 Buckling under compressive loads

The buckling of a flagpole under its own uniformly-distributed weight was solved by den Hartog using Vianello's method [4] and a similar, but more accurate, solution was given by [12]

$$w_{\text{crit}} = 7.837 \frac{EI}{L^3} \quad (3.1)$$

Figure 3.1 presents the normalized buckling load for several meshes (number of elements of equal length varied). The convergence of the critical load is apparently to a number slightly different from that of (3.1). The difference is less than .1%.

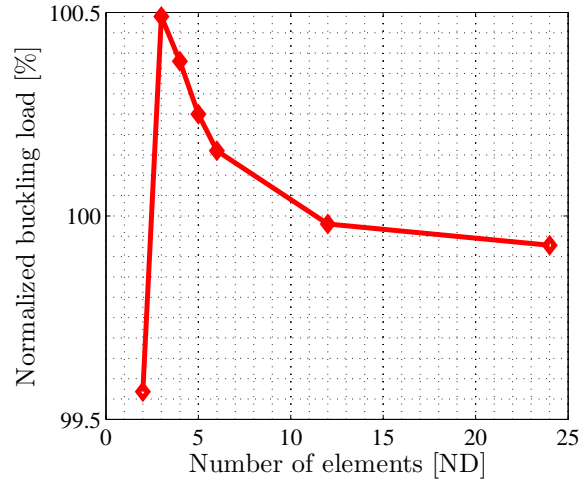


Fig. 3.1. Flagpole under own weight. Buckling load normalized by (3.1)

3.1.2 Torsional buckling

Torsional buckling of shafts with circular cross-section was addressed computationally by Argyris et al. [2]. The table 3.1 lists the various combinations of the support conditions and the ways in which the torsion is applied (axially, semi-tangentially, and quasi-tangentially).








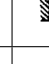

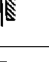
	Support conditions				
					
Torque application					
Axial	2.861	2	—	—	—
Semi-tangential	—	—	1	2.168	1.564
Quasi-tangential	—	—	0.5	1.576	1 (parallel), 1.021 (orthogonal)

Table 3.1. Buckling of shafts with circular cross-section of radius R . Critical load factors λ for various support conditions and moment applications, $M_{cr} = \pm \lambda \pi (E \pi R^4 / 4) / L$.

Figures 3.2 – 3.6 and illustrate the results obtained with the present model. Both the first-order and the second-order geometric stiffness matrices yield identical buckling factors. The apparent inaccuracy for the clamped-clamped conditions for a two-element model is simply due to the inability of such coarse model to represent the positive and negative curvature required in these cases within a single element; otherwise the convergence is evidently rapid.

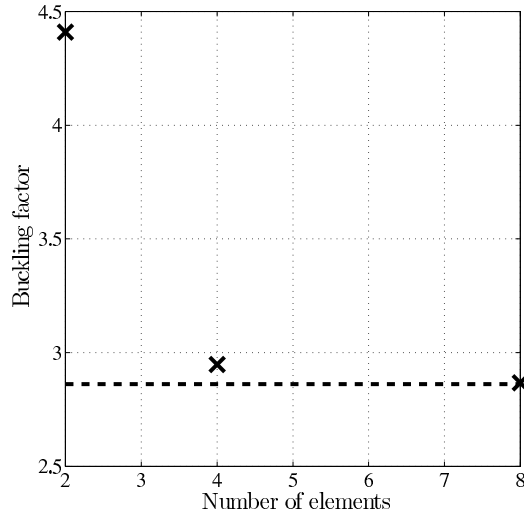


Fig. 3.2. Shaft with a circular cross section, clamped-clamped support. Convergence of the critical torque.

3.2 Modal analysis

3.2.1 Torsional vibration of drill pipe with collar

The first two natural torsional frequencies of an oil-well drill pipe are to be determined. The pipe is considered fixed at the upper end and terminates at the lower end by a drill collar with a given torsional mass inertia. The drill collar length is small compared to the pipe length.

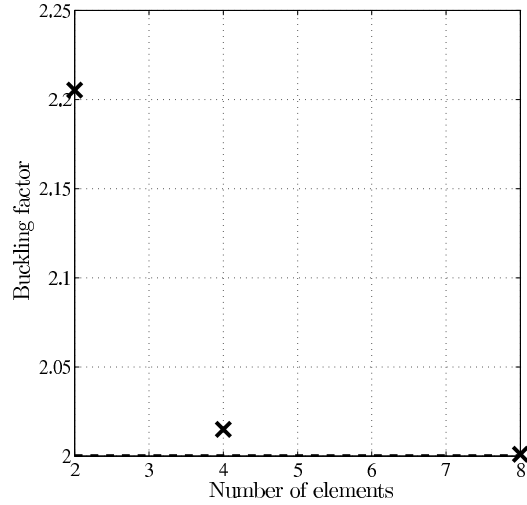


Fig. 3.3. Shaft with a circular cross section, clamped-sliding clamped support. Convergence of the critical torque.

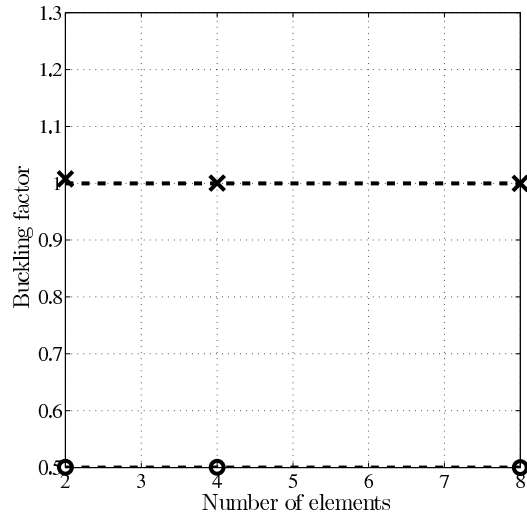


Fig. 3.4. Shaft with a circular cross section, clamped-free support. Convergence of the critical torque. Semi-tangential moment: X symbol; quasi-tangential moment: O symbol.

The data are given as follows: shear modulus $G = 12 \times 10^6$ psi, Poisson ratio 0.3, mass density $\rho = 15.2174 \text{ lb} - \text{sec}^2/\text{ft}^4$, length of the drill pipe $L = 5000$ ft, internal/external diameter of the pipe 4.5/3.83 in, and mass moment of inertia of the collar $I_p = 9.226 \times 10^{-4} \text{ ft}^4$.

The mesh was constructed to consist of 12 degrees of freedom (torsion only). The results are summarized in Table 3.2. The analytical solution and the numerical solution obtained with Ansys compares closely with present results.

Source	Frequency 1 [Hz]	Frequency 2 [Hz]
Analytical	0.3833	1.260
Ansys	0.3834	1.264
Present	0.3834	1.264

Table 3.2. The first two torsional natural frequencies of drill pipe with massive collar.

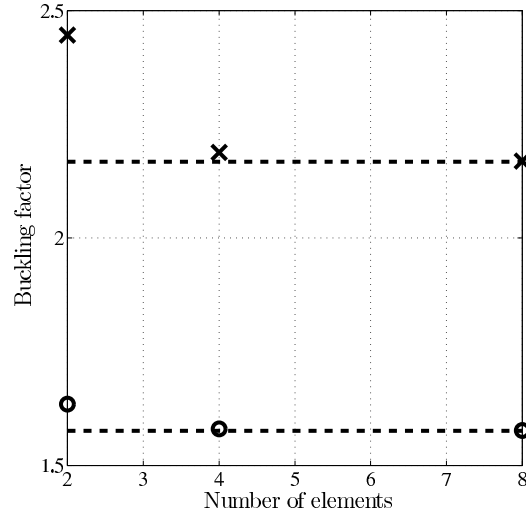


Fig. 3.5. Shaft with a circular cross section, clamped-simple support. Convergence of the critical torque. Semi-tangential moment: X symbol; quasi-tangential moment: O symbol.

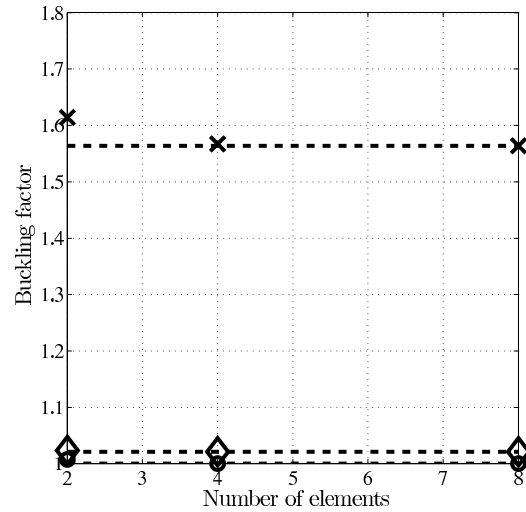


Fig. 3.6. Shaft with a circular cross section, simple-simple support. Convergence of the critical torque. Semi-tangential moment: X symbol; quasi-tangential moment (parallel levers at the top and bottom): O symbol; quasi-tangential moment (perpendicular levers at the top and bottom): ◇ symbol.

3.2.2 Axially prestressed column

The axially compressed beam (column) both before bifurcation of equilibrium (straight) and after buckling (bent) was studied for instance by Lestari and Hanagud [9]. Here we study a simply-supported beam/column both without transverse load (just axial compression) and with transverse load.

The beam has rectangular cross section of 0.25×4 in and length of 24in. The material parameters are those of steel (Young's modulus $E = 2.9 \times 10^4$ ksi, Poisson ratio $\nu = 0.3$, and mass density $\rho = 0.28 \text{ lbm} \cdot \text{in}^{-3}$).

The problem is investigated as follows: the static equilibrium under the applied loads (axial force only, or axial force plus transverse load) is found by solving the nonlinear equilibrium equations. Then the free vibration problem for small-amplitude superimposed oscillation (2.94) is solved where the tangent stiffness matrix incorporates the pre-stress due to all applied loads.

Consider first the beam with only the axial force. It is expected that the structure will experience bifurcation of equilibrium at the axial load being equal to the Euler buckling load. The three lowest frequencies of free vibration are found for various values of axial force P , both tensile and compressive. P_{Euler} is the Euler buckling load of a perfectly straight column. The natural frequencies are normalized as

$$\text{sign}(\omega_k^2(P/P_{Euler})) \frac{|\omega_k(P/P_{Euler})|}{\omega_1(0)}. \quad (3.2)$$

Here $\omega_1(0)$ is the analytically determined lowest frequency of free vibration of a simply-supported beam without axial load ($P/P_{Euler} = 0$). Note that the normalization includes the possibility of the natural frequencies becoming imaginary, so that $\omega_k^2(P/P_{Euler}) < 0$ is possible. This can occur when the structure attains unstable equilibrium.

As shown in Figure 3.7, the first frequency is equal to the analytically determined lowest frequency of free vibration of a simply-supported beam without axial load for $P/P_{Euler} = 0$. The first natural frequency drops to zero when the axial load is compressive and equal to the Euler buckling load, and becomes imaginary (so that the normalized frequency is negative) for compressive loads above the buckling load. In these situations the beam is still straight in equilibrium, but that equilibrium is unstable since the bifurcation associated with the Euler buckling load was passed.

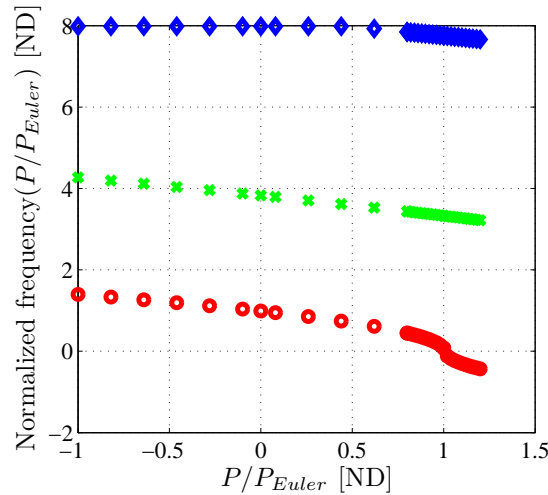


Fig. 3.7. Axially loaded beam/column. No transverse load. The first three natural frequencies normalized by the lowest natural frequency of beam without axial load, $\text{sign}(\omega_k^2(P/P_{Euler}))|\omega_k(P/P_{Euler})|/\omega_1(0)$.

Consider next the beam with axial force and uniform transverse load. In this case it is expected that the structure will assume a bent configuration for any value of the axial load, but at the axial load being close to the Euler buckling load and above the transverse deflection sharply increases. The beam in the bent configuration is always stable.

As shown in Figure 3.8, the first frequency is equal to the analytically determined lowest frequency of free vibration of a simply-supported beam without axial load for $P/P_{Euler} = 0$. The first natural frequency approaches zero when the axial load is compressive and close to the Euler buckling load but never actually becomes zero. For compressive loads above the buckling load the lowest frequency start increasing again because of the increase in the transverse deflection. It is interesting to observe the effect of the axial load upon the second and third lowest frequency of vibration which experience a sharp drop.

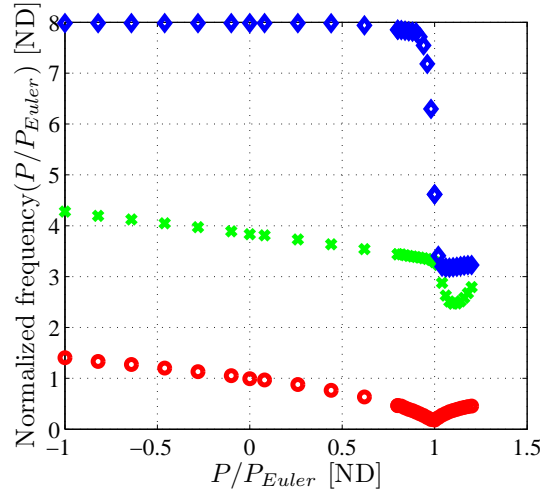


Fig. 3.8. Axially loaded beam/column with transverse load. The first three natural frequencies normalized by the lowest natural frequency of beam without axial load, $\text{sign}(\omega_k^2(P/P_{Euler}))|\omega_k(P/P_{Euler})|/\omega_1(0)$.

3.3 Static large-deflection analysis

3.3.1 Circular-arc cantilever

The structure is a circular-arc cantilever, clamped at one end and loaded with a vertical force $P = 600$ at the other end. The material properties are: Young's modulus 10^7 , zero Poisson's ratio. The radius is $R = 100$, and a cross-section of 1×1 units. The ABAQUS solution [1] is reported for a mesh of eight B31 beam elements as $u_x = -13.62$, $u_y = -23.78$, $u_z = 53.58$. The reference solution was taken from the paper of Izzuddin and Elnashai [10], but the structure was studied by many other researchers. Figure 3.9 shows the model and one computational mesh in the undeformed and final deformed state.

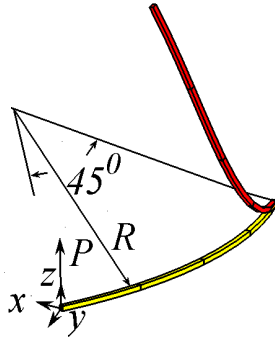


Fig. 3.9. Curved cantilever, four-element mesh. Undeformed and final deformed shape.

Figure 3.10 shows the tip displacements obtained for eight finite elements. Agreement with the reference solutions is rather close. For the final value of the load the present model obtained the tip deflection $u_x = -13.97$, $u_y = -24.16$, $u_z = 53.78$.

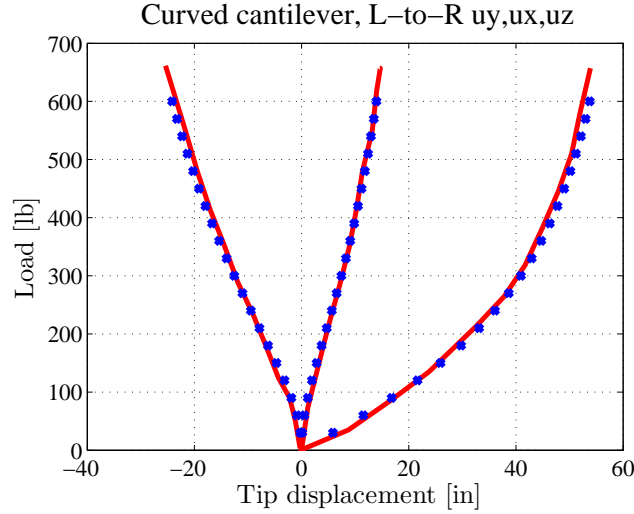


Fig. 3.10. Curved cantilever. Reference solution solid red line, present results shown by O symbol.

3.4 Transient vibration

3.4.1 Beam with time-dependent axial force

The simply supported beam with axial force that has harmonically varying time-dependent component is a classical parametric-resonance instability problem [12]. The applied force is

$$P(t) = P_{\text{Euler}} (p + s \cos \Omega t) , \quad (3.3)$$

where $0 \leq p$ is the time invariant component, and s is the multiplier of the harmonically varying component, and P_{Euler} the static Euler buckling load.

The beam considered here is of rectangular cross-section 6×60 mm and length of 1300 mm. The material properties of aluminum were: Young's modulus 71240 MPa, Poisson's ratio 0.31, and mass density $2700 \text{ kg} \cdot \text{m}^{-3}$.

In order to generate transverse vibrations the beam was considered pre-curved with imperfection equal to 0.6 mm at midspan. Three responses were computed for three sets of parameters that describe the stability diagram of Figure 3.11:

$$a = \frac{\omega_1^2}{\Omega^2} (1 - p) , \quad b = -\frac{\omega_1^2}{\Omega^2} s \quad (3.4)$$

Set 1 corresponds to a purely dynamic axial force applied at frequency equal to double the fundamental frequency of transverse vibration of the beam (Figure 3.12). The point (a, b) falls into the region of instability, and the figure clearly shows vibrations growing without bounds (the limits on the vertical axis correspond to about three times the thickness of the beam). Set 2 corresponds to a purely dynamic force, but at frequency that is mistuned by approximately 5% with respect to the frequency at which the first instability occurs. Therefore point 2 falls within a stability region, and Figure 3.13 is an evidence for stable, small-amplitude vibration. Set 3 corresponds to a total dynamic force which is periodically 50% in excess of the Euler buckling load. Yet point 3 falls within a stability region, and even though the amplitude of the vibration is considerable (on the order of half the thickness of the beam) it is stable (Figure 3.14).

3.4.2 Dynamics of spinning beams

The so-called Lagrange top is a well studied example of a spinning structure [7, 8]. Figure 3.15 illustrates the structure considered here: rectangular prism of square cross-section of 60 mm on the

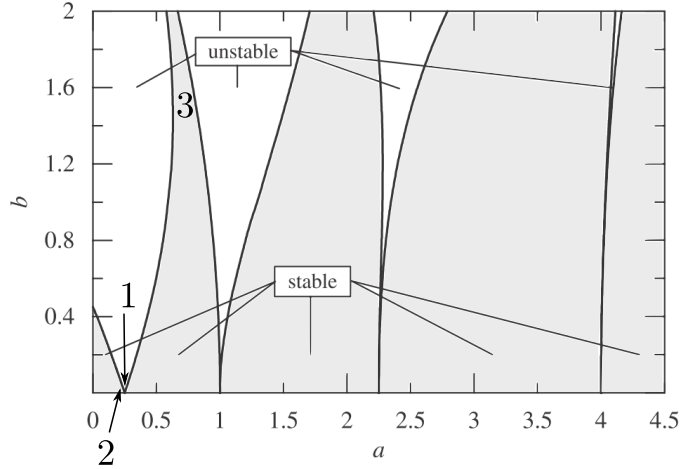


Fig. 3.11. Regions of stable and unstable solutions for the Mathieu equation.

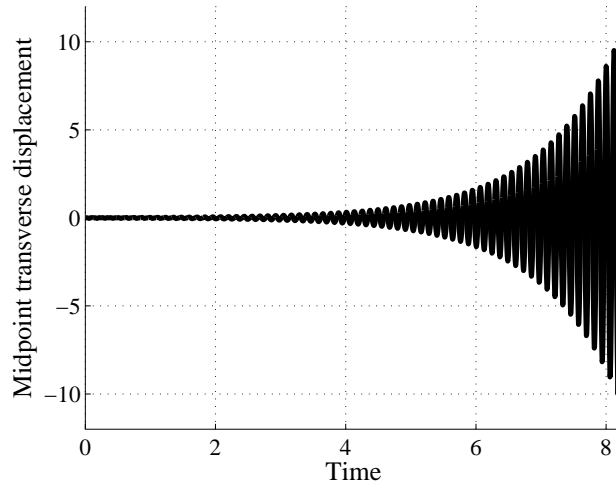


Fig. 3.12. Dynamically compressed pre-curved simply-supported beam. No static component, $p = 0$, dynamic component $s = -1/13$ tuned to the fundamental frequency of transverse vibration, $\frac{\omega_1^2}{\Omega^2} = 1/4$; the parameters in the stability diagram 3.11 are $a = 1/4, b = 0.0192$ (point 1).

side and length of 120 mm, made of aluminum (Young's modulus $E = 71240.0$ MPa, Poisson ratio $\nu = 0.31$, and mass density $\rho = 2700 \text{ kg} \cdot \text{mm}^{-3}$), and supported by a spherical joint at the origin of the Cartesian coordinates, is made to spin about its axis x_1 with an initial angular velocity Ω_0 . Gravitational acceleration $g = 9.81 \text{ m} \cdot \text{s}^{-2}$ is assumed to act against the positive z -axis.

First we show results for a “slow” top, with $\Omega_0 = 90\pi$, integrated on the time interval $0 \leq t \leq 2.8$ s. Figure 3.16 shows the motion of the tip of the unit vector \mathbf{v}_{CG} projected into the xy plane (see Figure 3.15). The red curve is the results of the simulation of the equations of motion of a rotating rigid body executed with a specialized time integrator [8] (momentum-conserving mid-point). Note that the magnitude of the motion of the projection of the unit vector tip indicates that the rotations of the top about the x and y axes are very large, of course in addition to the spin about the axis of the top.

Mesh of three beam elements of equal length was used with the Newmark algorithm running at time step $\Delta t = 2\pi/\Omega_0/100$, and every 25th step is shown with a marker. The agreement with the rigid-body simulation is excellent. Note that this agreement does not have been achieved without the inclusion of the gyroscopic matrix of Section 2.11.

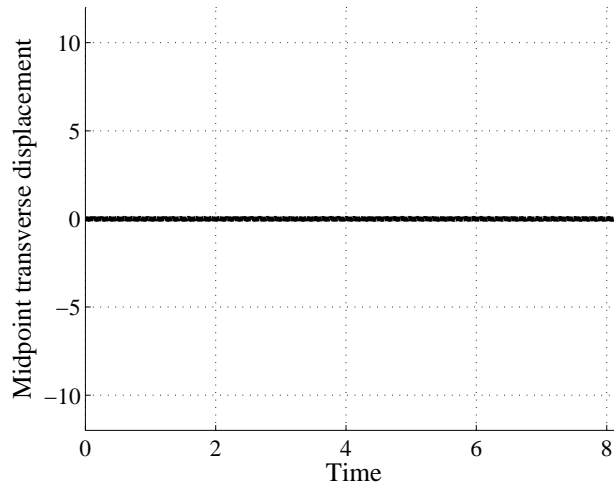


Fig. 3.13. Dynamically compressed pre-curved simply-supported beam. No static component, $p = 0$, dynamic component $s = -1/13$ mistuned with respect to fundamental frequency of transverse vibration, $\frac{\omega_1^2}{\Omega^2} = 0.2268$; the parameters in the stability diagram 3.11 are $a = 0.2268, b = 0.0174$ (point 2).

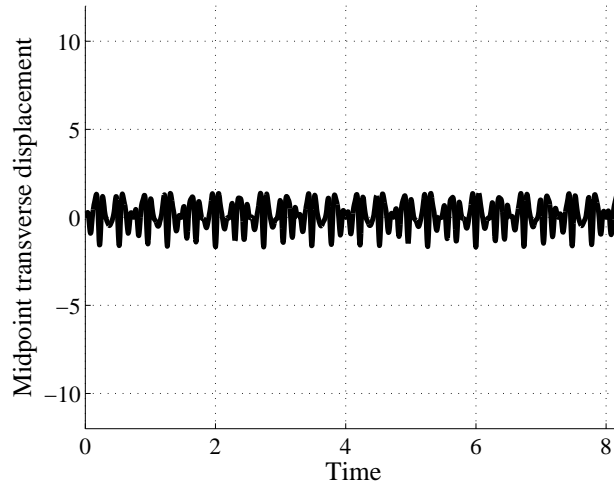


Fig. 3.14. Dynamically compressed pre-curved simply-supported beam. Static component, $p = 1/2$, dynamic component $s = -1.0$ at the frequency, $\frac{\omega_1^2}{\Omega^2} = 3/2$; the parameters in the stability diagram 3.11 are $a = 3/4, b = 3/2$ (point 3).

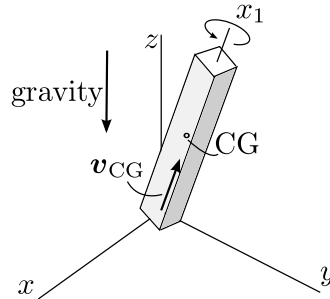


Fig. 3.15. Lagrange top. CG= center of gravity. The unit vector v_{CG} points from the spherical joint at the origin of the coordinates towards the center of gravity.

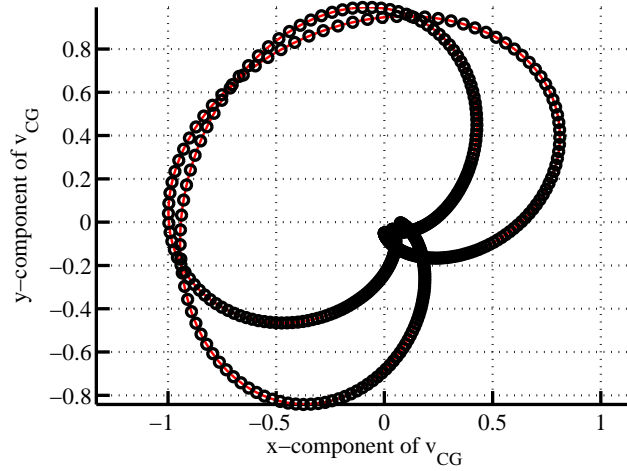


Fig. 3.16. Slow Lagrange top. Rigid-body simulation solid red line, beam model results shown by O symbol every 25 step. Consistent mass matrix.

Next we show results for a “fast” top, with $\Omega_0 = 313\pi$, integrated on the time interval $0 \leq t \leq 0.8$ s. Figure 3.17 shows the motion of the tip of the unit vector \mathbf{v}_{CG} projected into the xy plane (see Figure 3.15). The red curve is the results of the simulation of the equations of motion of a rotating rigid body as above for the slow top. Note that the magnitude of the motion of the projection of the unit vector tip indicates that the rotations of the top about the x and y axes are rather modest, but the spin about the axis of the top is substantial so that within the simulation the top executes approximately 125 revolutions.

Mesh of three beam elements of equal length was used with the Newmark algorithm running at time step $\Delta t = 2\pi/\Omega_0/10$, and every 20th step is shown with a marker. The agreement with the rigid-body simulation is quite good, and the match is improved by running at a shorter time step as shown in Figure 3.18, where the results were computed with time step $\Delta t = 2\pi/\Omega_0/50$. Again, realistic results required the inclusion of the gyroscopic matrix of Section 2.11.

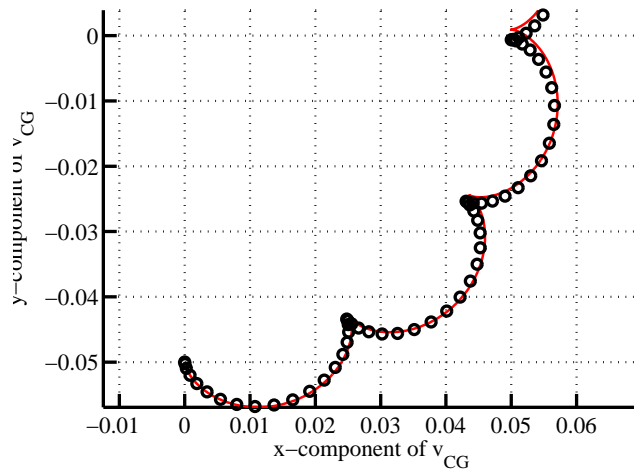


Fig. 3.17. Fast Lagrange top. Rigid-body simulation solid red line, beam model results for time step $\Delta t = 2\pi/\Omega_0/10$ shown by O symbol every 20 step. Consistent mass matrix.

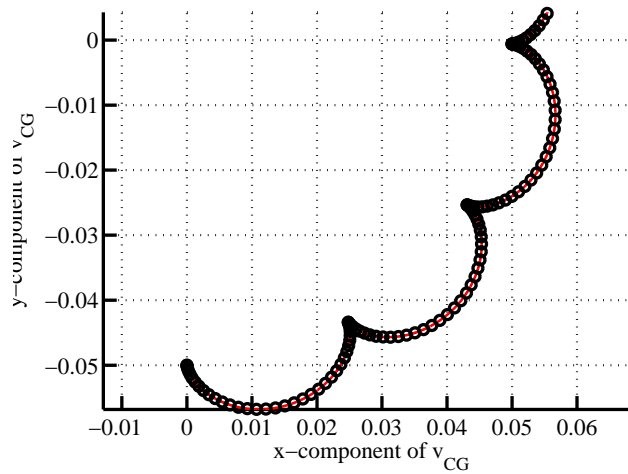


Fig. 3.18. Fast Lagrange top. Rigid-body simulation solid red line, beam model results for time step $\Delta t = 2\pi/\Omega_0/50$ shown by O symbol every 50 step. Consistent mass matrix.

3.4.3 Finite-amplitude dynamic deformation

The structure is an aluminum right-angle frame of rectangular cross-section 10×30 mm and length of both legs along the mid-line 240 mm (Figure 3.19). The material properties of aluminum were taken as: Young's modulus 71240 MPa, Poisson's ratio 0.31, and mass density $2700 \text{ kg} \cdot \text{m}^{-3}$.

The structure is supported by a spherical joint, and it is brought into motion by a force with a triangular shape in time applied at the elbow. Figure 3.19 demonstrates the magnitude of the motion by recording the deformed shape of the frame every 20th time step.

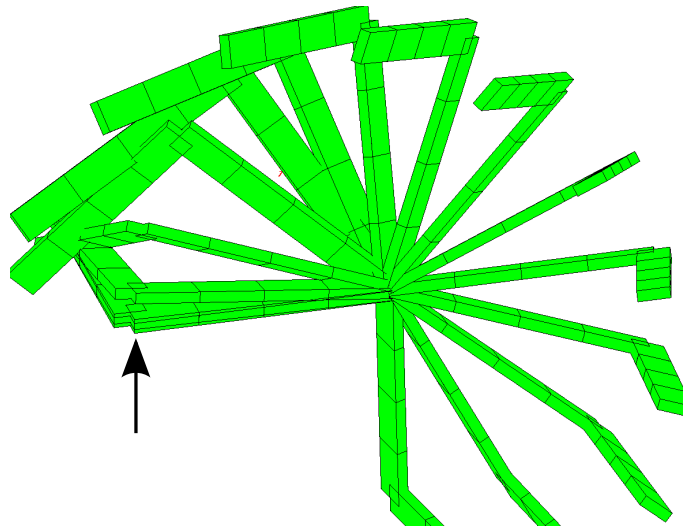


Fig. 3.19. Swinging aluminum frame. Snapshot of displacement every 20 steps. The impulse force at the elbow indicated by arrow.

The motion of the elbow and the free tip is shown in Figure 3.20. The beam model is verified by comparison with a fully nonlinear 3-D solid model. The solid model used the neohookean nonlinear

elasticity material formulation and 20-node hexahedra. The agreement of the beam solution with the fully three-dimensional reference solution is excellent.

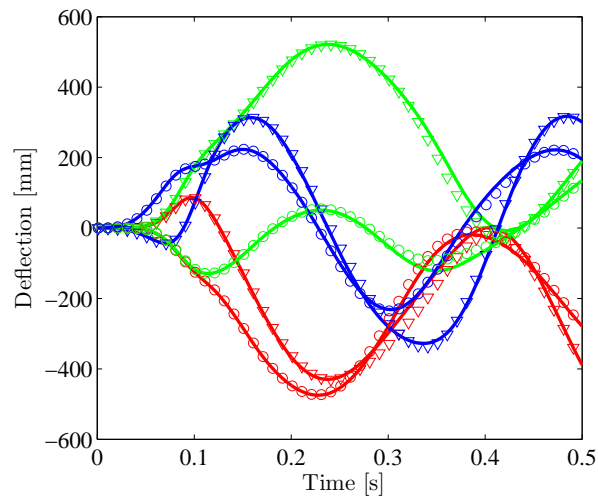


Fig. 3.20. Swinging aluminum frame. Solid lines are the reference solution with a fully nonlinear 3-D solid model. Symbols represent beam solution (\circ displacement of the elbow, ∇ displacement of the tip)). Red, green, blue = u_x, u_y, u_z .

References

1. ABAQUS, Inc. . *ABAQUS Verification Manual*, version 6.7 edition, 2007.
2. J. H. Argyris, P. C. Dunne, and D. W. Scharpf. Large displacement small strain analysis of structures with rotational degrees of freedom. *Computer Methods in Applied Mechanics and Engineering*, 14(3):401–451, 1978.
3. J. H. Argyris, O. Hilpert, G. A. Malejannakis, and D. W. Scharpf. Geometrical stiffness of a beam in space - consistent VW approach. *Computer Methods in Applied Mechanics and Engineering*, 20(1):105–131, 1979.
4. J. P. den Hartog. *Advanced strength of materials*. Dover Publications, Inc., 1987.
5. S. Krenk. *Non-linear Modeling and Analysis of Solids and Structures*. Cambridge University Press, 2009.
6. P. Krysl. *Nonlinear stability and large deflections of spatial structures with the finite element method*. PhD thesis, Czech Technical University in Prague, March 1993. In Czech.
7. P. Krysl. Explicit momentum-conserving integrator for dynamics of rigid bodies approximating the midpoint Lie algorithm. *International Journal for Numerical Methods in Engineering*, 63(15):2171–2193, 2005.
8. P. Krysl. Dynamically equivalent implicit algorithms for the integration of rigid body rotations. *Communications in Numerical Methods in Engineering*, 24(2):141–156, 2008. Krysl, P.
9. W. Lestari and S. Hanagud. Nonlinear vibration of buckled beams: some exact solutions. *International Journal of Solids and Structures*, 38(26-27):4741–4757, 2001.
10. B. A. Izzuddin I and A. S. Elnashai. Eulerian formulation for large-displacement analysis of space frames. *Journal of Engineering Mechanics*, 119(3), 1993.
11. S. S. Rao. *Mechanical vibrations*. Addison-Wesley publishing Company, 1990.
12. S. P. Timoshenko and J.M. Gere. *Theory of elastic stability*. Dover Publications Inc., 2 edition, 2009.
13. M. W. Wambsganss, S. S. Chen, and J. A. Jendrzejczyk. Added mass and damping of a vibrating rod in confined viscous fluids. Technical memorandum ANL-CT-75-08, Argonne National LaBarbera, 1974.